https://doi.org/10.5194/egusphere-2026-2309
Preprint. Discussion started: 20 May 2026

Constraints on NO_x emission in Thailand using GEMS satellite data

Worapop Thongsame[1,3], Daven K. Henze[1], Gabriele Pfister[2], Rajesh Kumar[2], Mary Barth[2]
[1]Paul M. Rady Mechanical Engineering, University of Colorado Boulder, Boulder, CO 80309, USA
[2]National Science Foundation, National Center for Atmospheric Research, Boulder, CO 80301, USA
[3]Center for Atmospheric Science Research, National Astronomical Research Institute of Thailand, Chiang Mai 50180, Thailand

Correspondence to: Worapop Thongsame (t.worapop@gmail.com)

Abstract

Nitrogen oxides (NO_x = NO + NO_2) are key pollutants that contribute to ozone and secondary aerosol formation, posing environmental and health risks. Accurate simulation and forecasting of NO_x pollution is essential for developing mitigation strategies. Local inventories in Thailand are infrequently updated, leading researchers to use global inventories such as CAMS-GLOB-ANT for simulation. Global inventories carry uncertainties due to assumptions in emission factors, outdated activity data, and coarse temporal resolution. To address these limitations, this study applies a top-down approach to update NO_x emissions in Thailand using the iterative finite difference mass balance (IFDMB) method. Tropospheric NO_2 vertical column densities (VCDs) from the GEMS are integrated with the WRF-Chem to refine CAMS-GLOB-ANT emissions for September 2023. The simulations with posterior emissions are evaluated against TROPOMI NO_2 VCDs and surface NO_x concentration. Results show that the baseline simulation overestimates NO_2 VCDs across Thailand compared with GEMS, except in North Thailand. Consequently, IFDMB reduces NO_x emissions across most regions but increases in the North. These adjustments improve model bias and error relative to GEMS. However, when evaluated against TROPOMI, we find an increase in the bias for North Thailand, likely due to discrepancies between GEMS and TROPOMI retrievals. Discrepancies between GEMS and TROPOMI highlight the importance of future calibration across satellite products. Comparisons to surface observations indicate that IFDMB shifts the NO_x peak to later than observations. This is because observations are strongly influenced by local transportation sources, which are hard to observe and simulate by GEMS and the model, respectively.

1. Introduction

Nitrogen oxides (NO_x = NO_2 + NO) are significant air pollutants that impact both the environment and human health. In the atmosphere, the suite of NO_x chemical reactions can lead to the formation of aerosol nitrate and ozone, worsening air quality (Adams et al., 2001; Philip et al., 2014; Thompson, 1992). The atmospheric deposition of NO_x products and its potential for oxidation contribute to the acidification of soil (Zhang et al., 2012). For human health impacts, long-term exposure to NO_x is associated with increased mortality rates due to respiratory issues and cardiovascular diseases (Eum et al., 2022; Ji et al., 2015). In Thailand, 10% of adult mortality in 2009 is attributable to NO_2 exposure (Pinichka et al., 2017). The primary sources of NO_x are anthropogenic, mainly from the combustion of fossil fuels in automobiles, power plants, and industrial activities (Cooper et al., 2017; Delmas et al., 1997). In urban areas of Thailand, such as Bangkok, vehicle emissions are the primary contributors to

https://doi.org/10.5194/egusphere-2026-2309
Preprint. Discussion started: 20 May 2026

NO_x levels (Uttamang et al., 2018). Conversely, in suburban areas like Rayong, the main sources of NO_x emissions are industrial activities (Poboon et al., 2012; Thawonkaew, 2016).

Ground-based monitoring stations provide highly accurate measurements of hourly NO_x mixing ratios; however, their spatial coverage is limited (Jeong and Hong, 2021). Moreover, NO_x highly depends on localized sources (Crippa et al., 2023; Miyazaki et al., 2017) and has a short atmospheric lifetime (Horner et al., 2024), leading to sharp spatial gradients and strong heterogeneity in ambient concentrations (Li et al., 2023). As a result, chemical transport models (CTMs) have become a widely adopted approach for studying NO_x and its impact on ozone as well as aerosol (Chen et al., 2013; Kim et al., 2024; Opio et al., 2022). Accurate simulation and forecasting of NO_x concentrations require accurate anthropogenic emission inventories (Miyazaki et al., 2017). Traditionally, anthropogenic emissions are developed from a bottom-up method, i.e., using emission factors and activity data to generate emissions (Cooper et al., 2017; Crippa et al., 2023; Ding et al., 2017). However, this approach often introduces significant uncertainties due to assumptions made regarding emission factors and activity data (Martin et al., 2003). Furthermore, bottom-up inventories take time to collect, prepare, and process, making them potentially outdated in rapidly changing regions (Ding et al., 2017; Lamsal et al., 2011; Liu et al., 2016). Alternatively, top-down methods, which leverage satellite data, provide potentially more accurate and near-real-time emissions (Lin et al., 2010; Yang et al., 2021).

Over the past two decades, various inverse methods using satellite observation to provide top-down emissions have emerged, such as Kalman filters, 4D-VAR, and mass balance (Cooper et al., 2017; Miyazaki et al., 2017; Napelenok et al., 2008; Qu et al., 2019). Among these, the mass balance method requires lower computational intensity for top-down emission constraining (Cooper et al., 2017; De Foy et al., 2014). This method is particularly effective for near-real-time updating of emissions using satellite observations (Lamsal et al., 2011). For constraining NO_x emissions, the mass balance method assumes a linear relationship between observed NO_2 vertical column density (VCD) and top-down NO_x emissions within a model grid cell, an assumption based on negligible horizontal transport when the lifetime of NO_x is short relative to the average transport time across a single grid cell of the model (Martin et al., 2003). However, NO_x can still disperse to adjacent grid cells, especially given the higher resolution of more contemporary air quality models, leading to a smearing error (Cooper et al., 2017). This error results in underestimations of emission changes at the source and can erroneously overestimate changes in downwind regions (Turner et al., 2012). An iterative approach has been proposed to address this issue by progressively shifting the adjustment from neighboring grid cells toward actual sources through repeated updates (Ghude et al., 2013). Additionally, the relationship between NO_x emission and NO_2 VCDs is non-linear due to non-linear chemistry (Jena et al., 2015). The finite difference mass balance method has been developed to account for the non-linearity between emissions and NO_2 VCDs (Cooper et al., 2017; Li et al., 2019). This improves accuracy by accounting for the sensitivity of changes in NO_2 VCDs to emissions, thus providing a refined tool to tackle the challenges associated with the smearing problem (Lamsal et al., 2011).

https://doi.org/10.5194/egusphere-2026-2309
Preprint. Discussion started: 20 May 2026

For the past few decades, NO_2 monitoring has relied on sun-synchronous Low Earth Orbit (LEO) satellites (e.g., GOME, SCIAMACHY, OMI, and TROPOMI) that provide a global map of tropospheric NO_2 (Boersma et al., 2008; Martin et al., 2003; Tang et al., 2013). However, LEO satellites have limited temporal sampling, which can miss rapid changes or diurnal patterns of NO_2 (Kim et al., 2023b). To address the challenges in data availability, Geostationary Earth Orbit (GEO) satellites, which have higher temporal and spatial resolution than the LEO satellite, have been launched (Choi, 2018; Seo et al., 2024; Yang et al., 2023). The Geostationary Environment Monitoring Spectrometer (GEMS) is a GEO satellite for air quality monitoring from space, providing unprecedented temporal resolution and continuous observational capabilities that are not feasible with LEO satellites (Kim et al., 2023a). This satellite is designed to measure air pollutants, including NO_2, sulfur dioxide (SO_2), formaldehyde (HCHO), and aerosols, over Asia (Kim et al., 2020). The hourly NO_2 data from GEMS can provide improvement for anthropogenic emissions (Park et al., 2023) and information about NO_2 diurnal variability (Park et al., 2024).

In this study, we explore the potential of GEMS satellite data for updating anthropogenic NO_x emissions over Thailand. Given the significant health impacts associated with NO_x exposure, accurate simulations are essential for developing effective mitigation policies. However, the lack of a local emission inventory poses a major limitation. Hence, our objective is to improve the accuracy of NO_x emissions used in air quality models and to assess diurnal variations in emissions. We employ a series of mass balance methods for adjusting anthropogenic NO_x emissions and utilize WRF-Chem to simulate NO_x concentrations in Thailand. The analysis focuses on September 2023—a period characterized by minimal biomass burning—allowing a clearer evaluation of anthropogenic emission contributions.

2. Methodology

2.1 WRF-Chem

We use the Weather Research and Forecasting model coupled with Chemistry (WRF-Chem) version 4.2.2 (Fast et al., 2006; Grell et al., 2005) to simulate NO_x concentrations over Thailand. The model domain and configuration, including grid nudging, largely follow Thongsame et al. (2024). The MOZART-MOSAIC with aqueous phase chemistry (Emmons et al., 2010; Knote et al., 2014; Zaveri et al., 2008) scheme is used for chemical and aerosol schemes. This scheme includes interactions of the aerosols with radiation and clouds. The online MEGAN version 2.04 (Guenther et al., 2006) and offline FINN versions 2.5 (Wiedinmyer et al., 2023) are used to represent biogenic and biomass burning emissions, respectively. Anthropogenic emissions are taken from the CAMS-GLOB-ANT v5.3 inventory (Granier et al., 2019), and the initial and boundary conditions come from the Whole Atmosphere Community Climate Model (WACCM; Granier et al., 2019). Figure 1 shows the distribution of NO_x emissions from CAMS-GLOB-ANT.

The simulation employs 42 vertical layers extending to approximately 63 hPa, with a horizontal resolution of 9 × 9 km^2. The model tropopause is located at approximately 100 hPa. To compare with GEMS, WRF-Chem NO_2 concentrations are interpolated to GEMS vertical pressure levels. Tropospheric NO_2 VCD from WRF-Chem is then calculated by integrating NO_2 from the surface to the GEMS-defined tropopause at 230 hPa. The GEMS averaging kernel is applied to the

https://doi.org/10.5194/egusphere-2026-2309
Preprint. Discussion started: 20 May 2026

model-simulated NO_2 profiles to account for the satellite's retrieval sensitivity, following previous approaches (Cooper et al., 2020; Park et al., 2024).

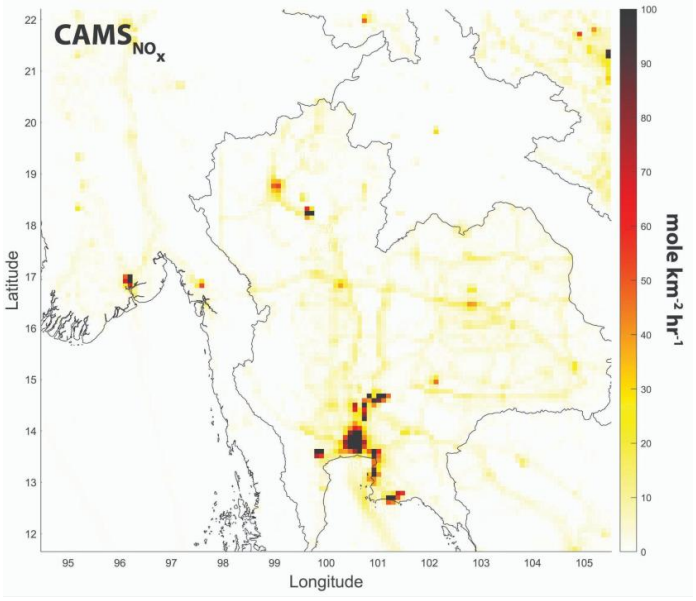

Figure 1: Spatial distribution of NO_x emissions from CAMS-GLOB-ANT in September 2023. BMR is the Bangkok Metropolitan Region.

2.2 GEMS

GEMS is an ultraviolet-visible instrument that measures back-scattered solar spectra in the 300–500 nm wavelength range (Kim et al., 2020). It is a geostationary orbit satellite, which was launched in February 2020, with a resolution of 3.5 × 8 km² (Kim et al., 2023a). The GEMS data span from November 2022 to the present, covering a geographical domain from 75°E to 145°E and 5°S to 45°N (Park et al., 2024). Tropospheric NO_2 VCDs are retrieved using a Differential Optical Absorption Spectroscopy (DOAS) algorithm, applied over the 432–450 nm spectral window (Kim et al., 2023a). Several studies have demonstrated strong correlations between GEMS NO_2 and ground-based measurements in regions such as China and South Korea (Kim et al., 2023a; Li et al., 2023; Seo et al., 2024).

For this research, we utilize version 3 of the GEMS Level 2 tropospheric NO_2 VCD (https://nesc.nier.go.kr/en/html/index.do) in September 2023 for the Thailand area. For September 2023, the dataset provides up to 10 consecutive hourly snapshots of tropospheric NO_2 VCD during daylight, from 00:45 to 07:45 UTC, with additional observations at 22:45 and 23:45 UTC.

For this analysis, we select data between 00:45–04:45 UTC and 06:45–07:45 UTC (07:45-11:45 and 13:45-14:45 local time), which collectively cover over 50% of Thailand. As the GEMS scan at 05:45 UTC does not extend to Thailand, the 05:45 UTC data are linearly interpolated from

https://doi.org/10.5194/egusphere-2026-2309
Preprint. Discussion started: 20 May 2026

adjacent hours (04:45 and 06:45 UTC) for updating the emission with the mass balance method. To ensure data quality, we retain only pixels with a cloud fraction below 0.3 (Park et al., 2024). We also filter data based on the final algorithm quality flag, a metric representing the reliability of each pixel's retrieval. Although a flag of 0 indicates an ideal measurement from the perspective of algorithmic issues, a systematic surface reflectance issue in GEMS version 3 prevents most pixels from achieving this score. Consequently, we use pixels with a quality flag of 0 or 1, ensuring sufficient data coverage while excluding severely degraded retrievals. Additionally, we have found striping artifacts present in the GEMS data (Fig. 2a). To ensure data quality and improve the reliability of the emission adjustment process, we manually remove these from our analysis. The data coverage in North Thailand is limited, and retrieval errors are relatively high in both North Thailand and the Bangkok Metropolitan Region (Figs. 2b and 2c). The tropopause pressure level used in GEMS retrievals is fixed at 230 hPa across all pixels.

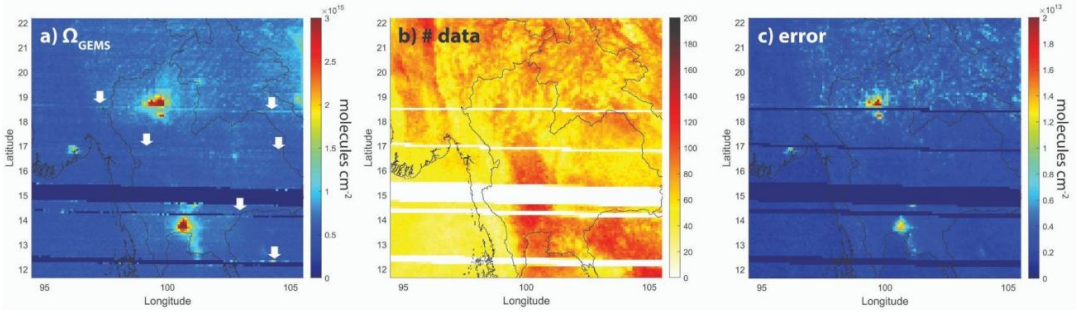

Figure 2: (a) Monthly average tropospheric NO_2 VCD in September 2023 from GEMS with arrows indicating striping artifacts. The number of GEMS data per grid cell (b) and (c) the monthly average error, σ_o, after removing striping artifacts.

2.3 TROPOMI

TROPOMI (TROPOspheric Monitoring Instrument) is a nadir-viewing UV–Visible spectrometer aboard Sentinel-5P that measures solar radiation backscattered from the Earth to retrieve atmospheric trace gases such as NO_2, O_3, SO_2, HCHO, CH_4, and CO (Judd et al., 2020; Veefkind et al., 2012). In this study, we use the Level 2 tropospheric NO_2 VCD product from TROPOMI version 2, which represents the NO_2 amount between the surface and tropopause. The TROPOMI tropospheric NO_2 retrieval uses a DOAS technique in the 405–465 nm spectral window, and its horizontal resolution is approximately 3.5 × 5.5 km^2 (Judd et al., 2020; Zhao et al., 2020).

For comparison with WRF-Chem simulations, we filter the TROPOMI data to retain only retrievals with a quality assurance value (qa_value) greater than 0.5, thereby excluding pixels affected by clouds, snow/ice, or retrieval artifacts. To ensure consistency in vertical sensitivity between the satellite and model data, we apply the TROPOMI-provided averaging kernels to the model-simulated NO_2 profiles. The TROPOMI satellite provides data around 10.30 am - 1.30 pm

https://doi.org/10.5194/egusphere-2026-2309
Preprint. Discussion started: 20 May 2026

local time for Thailand. The model outputs at the closest time to TROPOMI are used for comparison.

2.4 Ground-based monitoring data

For ground-based monitoring data, we use the data from the Pollution Control Department (PCD) of Thailand air quality stations (http://air4thai.pcd.go.th/webV3/) to evaluate surface NO_x concentrations from WRF-Chem. The PCD stations' measurements are based on the chemiluminescence technique, which detects NO_y species (Pollution Control Department, 2022; Zhang et al., 2009). Hence, we compare WRF-Chem NO_y (which includes NO_x and its oxidation products) with NO_x from PCD. The PCD stations (20) are classified into roadside (14) and non-roadside stations (6) as shown in Fig. S8.

2.5 Mass balance method

2.5.1 Finite difference mass balance

The mass balance method assumes a linear relationship between posterior NO_x emissions (E_t) and observed NO_2 columns (Ω_o) (Martin et al., 2003). This approach directly utilizes the information from the observed and simulated NO_2 columns, but does not account for the uncertainties associated with emissions or satellite retrievals (Cooper et al., 2017). The finite difference mass balance (FDMB) method, which integrates information from prior emissions, observations, and their uncertainties through a Bayesian inversion, is more robust and physically reasonable (Drinkwater et al., 2023; Watanabe et al., 2023). This method formulates a cost function, J, that penalizes deviations from observations and from prior emissions, and seeks the emissions that minimize J. The total cost function is defined as the sum of a prediction error term (model–observation mismatch) and an emission error term (departure from the prior emissions):

$$J = J_{prediction} + J_{parameter} \quad (1)$$

$$= \frac{1}{2}\frac{(\Omega_o-\Omega_a)^2}{(\sigma_o^2-C_1^2)} + \frac{1}{2}\frac{(E_t-E_a)^2}{(\sigma_a^2-C_2^2)} \quad (2)$$

where $J_{prediction}$ is the squared difference between observed and modeled NO_2 VCD, weighted by the uncertainty of the observation. The second term, $J_{parameter}$, penalizes large adjustments to the emissions from the prior, by squaring the difference between the optimized emissions E_t and prior E_a, weighted by the prior uncertainty. σ_o and σ_a are the observation and emissions errors, respectively. In this study, we assume a 50% relative uncertainty for the prior emissions based on previous studies (Jung et al., 2022; Park et al., 2024; Souri et al., 2020). The observation error is derived from the root mean square error (RMSE) in GEMS data. All of the terms in the above equation pertain to values in a single grid cell. The approach is applied independently across all grid cells in Thailand.

As σ_o is often quite low (on the order of 10% or less of Ω_o), the cost function in Eq. (2) can become overly sensitive to the prediction error term, potentially leading to overfitting. To prevent

https://doi.org/10.5194/egusphere-2026-2309
Preprint. Discussion started: 20 May 2026

this, we introduce a regularization term C_1 to inflate the denominator of the first term. In contrast, σ_a is significantly small in background areas, where emissions are close to zero. This leads Eq. (2) to become sensitive to the parameter error term and results in underfitting. Consequently, we add another regularization term C_2 in the second term. These regularization parameters effectively limit the influence of the prediction/parameter error term, thereby balancing the relative weights of the model–observation mismatch and the prior deviation terms. The low value of C_1 leads to overfitting the solution to observations, while the high value of C_1 leads to overfitting the solution to the prior, and vice versa for C_2. As σ_o and σ_a only quantify relative errors, the C_1 and C_2 terms can also be interpreted as absolute contributions to the total observation and emissions errors, respectively, such as a detection limit for the former. For the C values, we use 1x10^{14} molecules cm^{-2} for C_1 and 10 mol km^{-2} hr^{-1} for C_2. These numbers are based on the GEMS detection limit and background NO_x emission near the Bangkok area.

In this study, we use the analytic solution for the mass balance method from Cooper et al. (2017) for the FDMB method. To solve for posterior emission (E_t), we minimize the cost function in Eq. (3), and the updated emission as:

$$E_t = E_a + g(\Omega_o - \Omega_a) \quad (3)$$

where g is the gain factor that describes the sensitivity of the inversion to the observations (Ω_o) given the relative weighting of the uncertainties in emissions (σ_a) and in tropospheric NO_2 VCD (σ_o):

$$g = \frac{h\sigma_a^2}{h^2(\sigma_a^2 - C_2^2) + (\sigma_o^2 - C_1^2)} \quad (4)$$

where h is from Cooper et al. (2017):

$$h = \frac{\Omega_a}{\beta E_a} \quad (5)$$

In the above, h is a factor accounting for the sensitivity of the modeled NO_2 VCD change due to changes in emissions. β quantifies the sensitivity of the fractional change in the tropospheric NO_2 VCD to NO_x emissions (Lamsal et al., 2011),

$$\frac{\Delta E}{E} = \beta\left(\frac{\Delta\Omega}{\Omega}\right) \quad (6)$$

where ΔE is the difference between baseline and perturbed NO_x emissions, and $\Delta\Omega$ is the difference between the NO_2 VCD of WRF-Chem from baseline and perturbed NO_x emissions. As noted in Cooper et al. (2017), the magnitude of the emissions perturbation used for ΔE impacts the value of β. For stability, we apply a 10% perturbation to determine β, and we constrain β to be in the range of 0.1-10.

https://doi.org/10.5194/egusphere-2026-2309
Preprint. Discussion started: 20 May 2026

The form of g in Eq. (4) shows that if the prior uncertainty ($\sigma_a + C_2$) is large relative to the observational uncertainty ($\sigma_o + C_1$), the gain matrix g approaches 1, meaning the observations strongly influence the posterior emissions. Conversely, if the observations are very uncertain or the model is insensitive (small h), g becomes small, and the solution remains closer to the prior emissions (E_a). This Bayesian formulation thus provides a balanced update to emissions, taking into account both the reliability of the observations and the confidence in prior emission estimates.

2.5.2 Iteration

An iterative approach is applied to the finite difference mass balance methods. In this study, NO_x emissions are updated iteratively until the J is minimized. The sensitivity factor (β) is recalculated after each iteration to reflect changes in the NO_2 response to updated emissions. By continuously updating β, the method aims to better capture the prevailing NO_x chemical regime under the observed NO_2 column concentrations, rather than relying solely on sensitivities derived from the prior model state.

2.6 Experimental Design

Although IFDMB assumes negligible horizontal transport due to the short atmospheric lifetime of NO_2, our high-resolution simulations (9 x 9 km^2) violate this assumption, as there may be significant horizontal transport of NO_2 to surrounding grid cells. To mitigate the smearing error, we regrid both GEMS and WRF-Chem NO_2 VCDs to a coarser 81 × 81 km^2 resolution by spatially averaging over surrounding grid cells. To update NO_x emissions, we apply IFDMB in three different configurations: Fixed diurnal, Daylight diurnal, and Temporal average (Table 1). Each approach is described below. For each method, we use some form of a monthly average of the GEMS data to update emissions. This helps reduce the impact of noise and missing data in satellite observations. Additionally, the smearing error is minimized when considering monthly average NO_2 VCDs.

Table 1: Summary of emission update configurations and corresponding mass balance methods.

Update scheme	Update Scope	Diurnal Handling
Baseline simulation	No update	Thongsame et al. (2024)
Fixed diurnal	Full-day update	Thongsame et al. (2024)
Daylight diurnal	Daylight hours only	Updated daylight diurnal
Temporal average	Daylight hours only	3-hour temporal average for updated daylight diurnal

2.6.1 Fixed diurnal

For the fixed diurnal approach, we update monthly emissions without changing their diurnal variability. We calculate monthly averages of tropospheric NO_2 columns from both GEMS and WRF-Chem (at the satellite overpass times) during September 2023 (Fig. 3a). These monthly

https://doi.org/10.5194/egusphere-2026-2309
Preprint. Discussion started: 20 May 2026

averages are then used to compute a uniform scaling factor via each mass balance method (scaling factor$_{t=all}$). This scaling factor$_{t=all}$ is applied consistently to NO_x emissions at all time steps, including both daytime and nighttime hours. As GEMS provides data during daylight only, we assume the relative differences between GEMS and WRF-Chem are similar at all times.

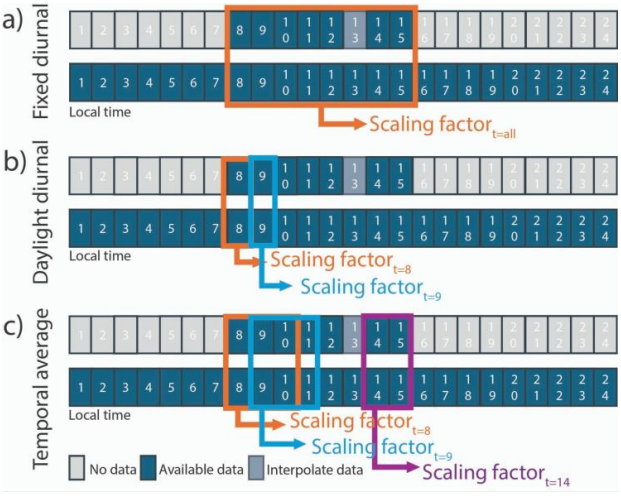

Figure 3: Schematic diagram explaining emission update configurations and corresponding mass balance methods: a) Fixed diurnal, b) Daylight diurnal, and c) Temporal average updates.

2.6.2 Daylight diurnal

Instead of monthly averaging, we compute the mean GEMS and WRF-Chem NO_2 VCDs for each GEMS scanning hour (Park et al., 2024). Specifically, the mean GEMS VCD at hour 08:00 comes from averaging GEMS data at 08:00 am every day in September 2023 (Fig. 3b). Hourly scaling factors are derived from these means and applied to emissions at the corresponding hour (scaling factor$_{t=8}$ at Fig. 3b). The emissions at the same hour are updated with the scaling factors of the same hour. This method captures the monthly diurnal variability of GEMS NO_2 and propagates it to the emission inventory. Since GEMS retrievals are only available during the daylight, emissions during nighttime hours remain unchanged. This update scheme takes advantage of the fact that that the lifetime of NO_x being generally relatively short. The NO_2 VCD at any given hour is impacted by emissions from that exact same hour. For example, NO_2 VCD at 08:00 is the result of emissions at 08:00, under the assumption that emissions from 06:00 or 07:00 have no residual impact on the NO_2 VCD at 08:00. We acknowledge this is a simplification; in reality, emissions take time to undergo chemical conversion (e.g., 08:00 emission peaking in NO_2 VCD around 08:15 - 08:30), and the emissions before 08:00 have impacts on NO_2 VCD at 08:00 due to the multiple hour lifetime of NO_x.

2.6.3 Temporal averaging

This method accounts for the persistence of NO_2 in the atmosphere, acknowledging that observed NO_2 VCDs at a given hour reflect not only current emissions but also emissions from prior hours (Park et al., 2024). Although NO_2 has a relatively short lifetime, it still spans several

https://doi.org/10.5194/egusphere-2026-2309
Preprint. Discussion started: 20 May 2026

hours. To address this, we assume that emissions affect NO_2 VCDs for up to two subsequent hours. For instance, NO_x emitted from a point source at 08:00 is assumed to contribute to the NO_2 VCDs measured at 08:00, 09:00, and 10:00. Therefore, the scaling factor for each hour is calculated from the average of NO_2 VCD at that hour and the following two hours every day in September 2023 (Fig. 3c). For example, the scaling factor for hour 08:00 is based on the mean NO_2 VCD observed at 08:00, 09:00, and 10:00 every day in September 2023 (scaling factor$_{t=8}$ at Fig. 3c). In the inverse method configuration, the average of NO_2 VCDs at 08:00, 09:00, and 10:00 is used rather than the 06:00 and 07:00 because the emissions have not emitted yet. This temporal smoothing better represents the time-integrated nature of NO_2 accumulation. For hours near the end of the GEMS window, such as 14:00 and 15:00, only two and one data points are used for the average, respectively. This is because there is only one subsequent data point from 14:00 and no subsequent data for 15:00. As the hourly scaling factors are calculated from monthly moving averages of data in each hour, the emissions at the same hour are updated with the same factors.

2.7 Evaluation method

Three metrics, namely, normalized mean bias (NMB), normalized root mean square error (NRMSE), and correlation coefficient (*R*), are used to evaluate the performance of the IFDMB solution in comparison to our simulation using the prior emissions. The σ_o from GEMS and TROPOMI is used to normalize bias and error. We compare our results with tropospheric NO_2 VCD from GEMS and TROPOMI, and with in situ NO_x measurements from PCD stations. For GEMS and TROPOMI, the monthly average tropospheric NO_2 VCDs in the Thailand grid cells are compared with the monthly average WRF-Chem results. This is because only emissions in Thailand are updated, while emissions outside Thailand remain the same. For PCD stations, we evaluate our results with MB, RMSE, and *R*, as the PCD stations have not reported the error of the instruments. Additionally, we compare the monthly average diurnal NO_x profile with PCD data.

3. Results and discussion

3.1 Comparison between baseline simulation and GEMS

This section shows the performance of the WRF-Chem simulation using the prior emissions (the CAMS-GLOB-ANT inventory), aka the baseline simulation, compared to GEMS NO_2 VCDs before applying any mass balance methods. Overall, the baseline simulation significantly overestimates the monthly average NO_2 VCDs in the Bangkok Metropolitan Region and East Thailand (Fig. 4). The baseline simulation shows that the NO_2 VCD is dominated by large point sources from many sectors. In North Thailand, the prior emissions identify the Mae Moh coal power plant (energy sector) as the main source of NO_2, with a signal that significantly overwhelms the urban emissions from Chiang Mai and Lampang (Fig. 1). In the Bangkok Metropolitan Region, the model suggests a mixed contribution from the dense residential and transportation sectors of the urban area. Additionally, industrial estates in Saraburi and Rayong produce high NO_2 – as strong as urban emissions in Bangkok. GEMS presents a contrasting picture that emphasizes the role of urban sources. In North Thailand, GEMS has the highest NO_2 VCDs centered over the urban areas of Chiang Mai and Lampang, which are dominated by residential and transportation emissions. The Mae Moh power plant appears as only a moderate

https://doi.org/10.5194/egusphere-2026-2309
Preprint. Discussion started: 20 May 2026

signal in the GEMS observations. This pattern holds in the Bangkok Metropolitan Region, where GEMS again highlights the urban area, while the signals from major industrial estates in Rayong and Saraburi are notably weaker than the urban emissions. Additionally, the GEMS NO_2 VCDs in North Thailand are as large as in the Bangkok Metropolitan Region, while the baseline simulation shows significantly larger NO_2 VCDs in the Bangkok Metropolitan Region. This direct contradiction between the baseline simulation and GEMS highlights that the CAMS-GLOB-ANT is likely to overestimate energy and industrial emissions relative to the residential and transportation emissions in Thailand. The baseline simulation shows high NMB and NRMSE in most regions, with comparatively better performance in North and West Thailand (Figs. 5 and S9). However, GEMS data availability is high in Central Thailand and the Bangkok Metropolitan Region, moderate in the North and East, and very limited in West Thailand (Fig. 2). The correlation coefficient is moderate (R = 0.65).

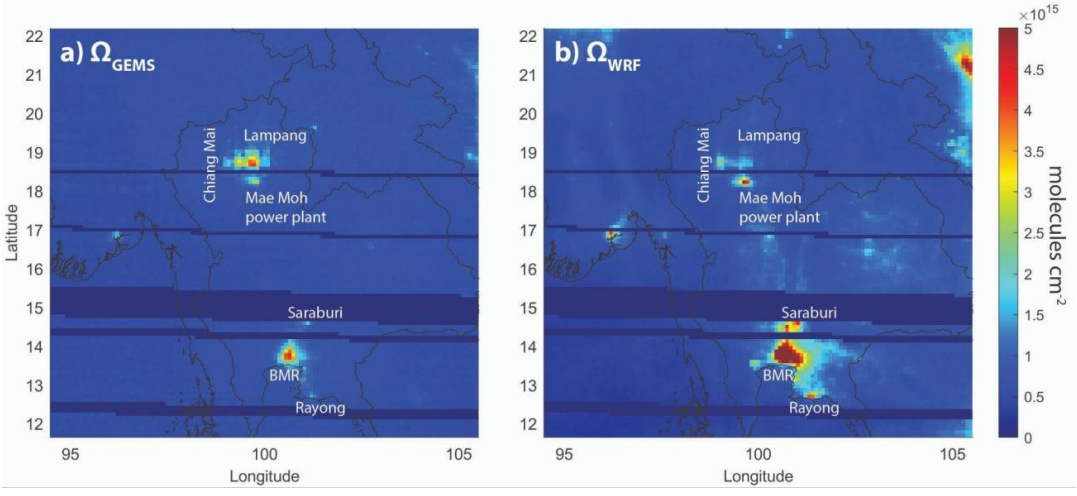

Figure 4: Monthly average tropospheric NO_2 VCD in September 2023 from GEMS (left) and the baseline simulation (right). High NO_2 VCDs are observed over urban areas such as Chiang Mai, Lampang, and the Bangkok Metropolitan Region (BMR), as well as over the Mae Moh power plant and industrial zones in Saraburi and Rayong.

https://doi.org/10.5194/egusphere-2026-2309
Preprint. Discussion started: 20 May 2026

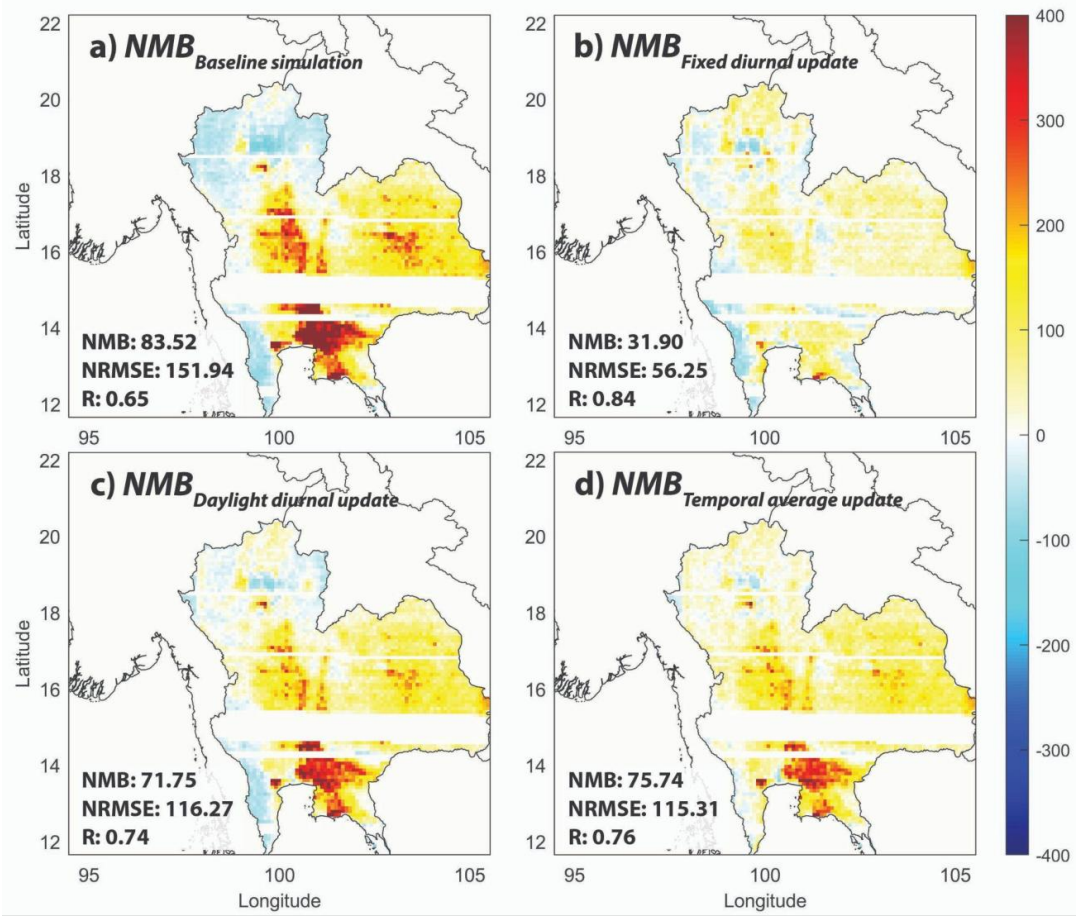

Figure 5: Spatial distribution of Normalized Mean Bias (NMB) of NO_2 VCD between WRF-Chem and GEMS of IFDMB for September 2023 using (a) prior emissions, and emissions updated by (b) fixed diurnal, (c) daylight diurnal, and (d) temporal average update schemes. Monthly statistical evaluations averaged across all grid cells in Thailand are provided for each simulation.

3.2 Evolution and optimization of mass balance methods

To determine the optimal number of iterations for the IFDMB inversion, we calculate the total cost function J, $J_{prediction}$, and $J_{parameter}$ based on comparisons between NO_2 VCDs from WRF-Chem and GEMS at each iteration (Fig. 6). Our results show that J decreases substantially during iterations 1 and 2 across all update schemes, but it begins to increase beyond iteration 3 (Fig. 5a). This increase in the total cost function is primarily driven by a rise in $J_{parameter}$ (Fig. 6c). The $J_{prediction}$ term slightly decreases after iteration 2. However, $J_{prediction}$ does not decrease monotonically due to overadjustment; it may increase in some iterations before decreasing again in subsequent steps (Fig. 6b). Our analysis shows that the daylight diurnal

https://doi.org/10.5194/egusphere-2026-2309
Preprint. Discussion started: 20 May 2026

scheme exhibits significant overadjustment because it assumes an immediate response of NO_2 VCDs to emission changes. For the fixed diurnal and daylight diurnal update schemes, iteration 2 provides the lowest J and is thus selected as optimal. For the temporal average update scheme, iteration 4 yields the optimal performance. Furthermore, analyses of the sensitivity of the cost function in the fixed diurnal scheme the parameters C_1, C_2, demostrate consistent model performance patterns across different parameter values (Sect. S1).

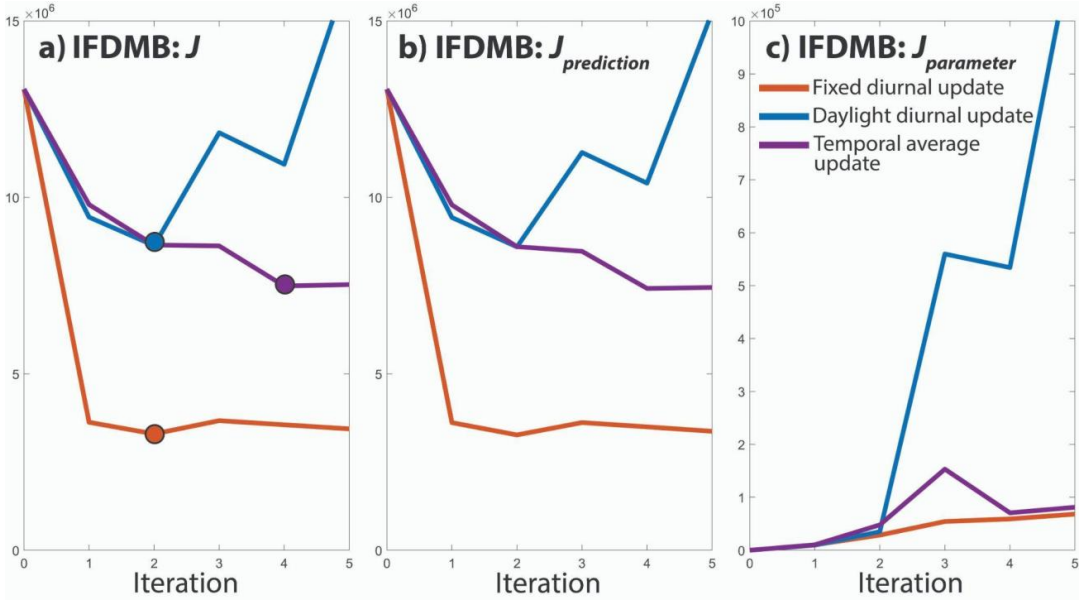

Figure 6: Evolution of the total cost function J (a), $J_{prediction}$ (b), and $J_{parameter}$ (c) over five iterations of IFDMB with three update schemes: fixed diurnal (orange), daylight diurnal (blue), and temporal average (purple). The optimal iteration for each scheme is marked with a filled circle.

3.3 Comparison with GEMS

This section presents the results from WRF-Chem simulations using the IFDMB method evaluated with GEMS. The IFDMB with all three update schemes reduces both NMB and NRMSE in GEMS compared to the baseline simulation (Fig. 5). The IFDMB with fixed diurnal update demonstrates the highest improvement among the three update schemes. The NMB and NRMSE reduce by about 60% for the fixed diurnal update. Reductions are most pronounced in Central Thailand and the Bangkok Metropolitan Region (Figs. 5 and S9). Overestimated NO_2 VCDs from transportation and residential sectors are substantially corrected. However, improvements in North and West Thailand are more modest. The improvement in those areas is limited due to the low data density and high errors in those areas. The correlation coefficient (R) improves from 0.65 (baseline simulation) to 0.84.

The IFDMB with daylight diurnal and temporal average updates produces similar results. Both methods improve the performance in urban areas, particularly in Bangkok and big cities in North Thailand, but are less effective in other areas (Figs. 5 and S9). The NMB is reduced by 14% for

https://doi.org/10.5194/egusphere-2026-2309
Preprint. Discussion started: 20 May 2026

the IFDMB with daylight diurnal update and 9% for the temporal average update. Notably, both updates exhibit small improvements during early morning hours (e.g., 8–9 AM) compared to the IFDMB with fixed diurnal update (Fig. S10). Since these methods only update emissions during the daylight, uncorrected nighttime emissions likely contribute to the error of NO_2 VCD in the early morning. In contrast, the fixed diurnal update, which adjusted emissions at all time steps, shows lower NMB and NRMSE throughout the day. The NRMSE reduction for these two methods is around 20% and correlation coefficients improve to 0.74 for the daylight diurnal update and 0.78 for the temporal average update.

3.4 Emissions updates

The use of GEMS satellite data to update NO_x emissions with the IFDMB method provides an increase in emissions in the North and West Thailand, while emission reductions are obtained in other areas (Fig. 7). The fixed diurnal update produces the largest emission adjustments, as it applies the scaling factor uniformly across all time steps, including periods with and without GEMS observations (Fig. 8). In this case, daily NO_x emissions increase approximately 20 mole km^{-2} hr^{-1} in North and West Thailand, while they decrease by about 30 mole km^{-2} hr^{-1} in other regions (Fig. 7). The IFDMB with daylight diurnal update, which only modifies emissions during hours with available GEMS data, results in the smallest overall changes. Increases and decreases are generally below 20 mole km^{-2} hr^{-1} across all regions (Fig. 7). The IFDMB with temporal average update produces similar results to the daylight diurnal update. However, the emission reduction in the Bangkok Metropolitan Region is stronger than the daylight diurnal update, with the reduction of about 30 mole km^{-2} hr^{-1}. A notable feature across all update schemes is the significant amplification of NO_x emissions in Lampang. This enhancement arises because the CAMS-GLOB-ANT inventory lacks representation of large point sources in that area, whereas GEMS indicates elevated NO_2 VCDs. Consequently, the IFDMB compensates for the discrepancy between simulated and observed NO_2 by intensifying the small prior emissions in Lampang.

For the diurnal variability, prior emissions follow almost the same diurnal profile across all regions in Thailand, depending on the dominant sectors. However, GEMS-informed updates reveal differences in diurnal variability across Thailand (Fig. 8). In Bangkok and North Thailand, the prior profile has a sharp morning peak between 08:00–09:00, followed by a flat midday period extending to 16:00. In contrast, both the IFDMB daylight diurnal and temporal average updates exhibit more dynamic variability, with pronounced peaks between 09:00–11:00 and a subsequent decline throughout the GEMS observation window in Bangkok. In North Thailand, the IFDMB daylight diurnal update peaks around 12:00 - 14:00, while the temporal average update peaks earlier, around 09:00 - 11:00. Our study reveals that the diurnal variability from Thongsame et al. (2023), which shows peaks aligned with morning and evening rush hours, is different from the GEMS diurnal variability. GEMS provides the potential to refine the diurnal variability during the daylight in Thailand. However, GEMS tends to underestimate NO_2 VCDs in the early morning and late afternoon, due to unfavorable viewing geometries during those times (Park et al., 2024). Future research is required to analyze this uncertainty and its impacts on diurnal variability.

https://doi.org/10.5194/egusphere-2026-2309
Preprint. Discussion started: 20 May 2026

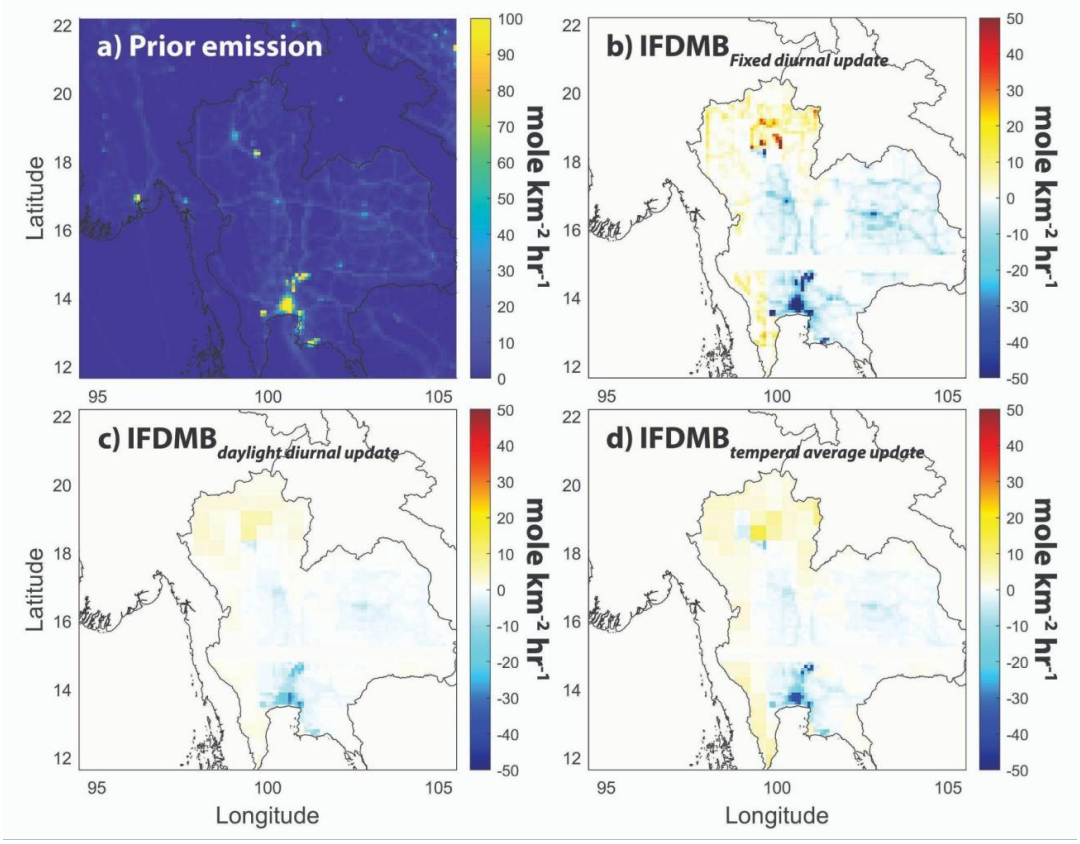

Figure 7: The change in monthly average NO_x emissions for the IFDMB compared to prior emissions: (a) prior emissions, (b) IFDMB with fixed diurnal update, (c) IFDMB with daylight diurnal update, and (d) IFDMB with temporal average update.

https://doi.org/10.5194/egusphere-2026-2309
Preprint. Discussion started: 20 May 2026

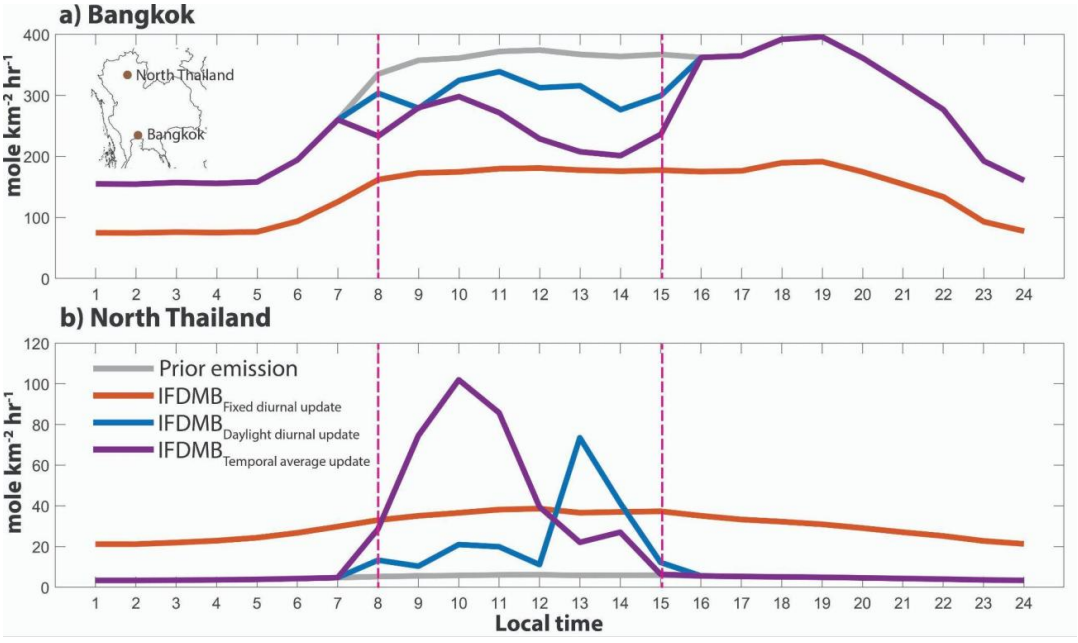

Figure 8: Hourly NO_x emissions averaged across nine grid cells in (a) Bangkok and (b) North Thailand comparing IFDMB with different update schemes: prior emission (gray), IFDMB with fixed diurnal update (orange), IFDMB with daylight diurnal update (blue), and IFDMB with temporal average update (purple). The pink line represents the GEMS window for Thailand.

3.5 Comparison with TROPOMI

In this section, we compare tropospheric NO_2 VCDs from the WRF-Chem simulations and GEMS with those from TROPOMI (Fig. 9). Because GEMS and TROPOMI differ in their averaging kernels and overpass times, a direct comparison is not feasible. Therefore, we focus on assessing the relative spatial distributions of NO_2. To ensure consistency, the GEMS and WRF-Chem VCDs closest to the TROPOMI overpass time are selected for comparison (Figs. 9c and 9d). The differences between the GEMS and TROPOMI overpass times are about 15 minutes. The monthly average GEMS NO_2 VCDs at the TROPOMI overpass times are slightly higher than the monthly average NO_2 derived from all GEMS observations (Figs. 9a and 9c). Moreover, they exhibit increased noise, particularly over rural areas. Overall, both satellites show similar spatial patterns of NO_2, except in North Thailand. High NO_2 is consistently observed in the Bangkok Metropolitan Region, Saraburi, and Rayong from both GEMS and TROPOMI. In North Thailand, both satellites detect high NO_2 associated with the Mae Moh power plant; however, GEMS shows anomalously high NO_2 over Lampang that is not observed by TROPOMI (Figs. 9c and 9e). The NO_2 levels in Lampang from GEMS exceed those in Bangkok, whereas TROPOMI indicates the highest NO_2 over the Bangkok Metropolitan Region. Additionally, TROPOMI generally has higher background NO_2 levels compared to source regions. To further examine the magnitude differences, we apply the respective averaging kernels of GEMS and TROPOMI to the baseline simulation. The results indicate that TROPOMI

https://doi.org/10.5194/egusphere-2026-2309
Preprint. Discussion started: 20 May 2026

retrieves higher NO_2 VCDs than GEMS across most regions, except in Lampang, where GEMS values remain substantially larger (Figs. 9d and 10f).

Our baseline simulation overestimates tropospheric NO_2 VCDs across Thailand relative to TROPOMI satellite observations (Figs. 9e and 9f). The model predicts strong NO_2 VCD from energy, industry, transportation, and residential sectors almost everywhere, whereas TROPOMI detects high NO_2 only in specific areas. In particular, TROPOMI shows high NO_2 only over the Bangkok Metropolitan Region (attributed largely to residential emissions) and at certain major point sources (e.g., the Mae Moh power plant in the North and large industrial zones in Central Thailand). Most other areas, including city centers in North and Northeast Thailand, exhibit only moderate NO_2 VCDs in the TROPOMI data. Additionally, TROPOMI shows moderate to low NO_2 along the major roads in Thailand, whereas the baseline simulation shows clear NO_2 enhancements. The monthly NMB from the baseline simulation is 0.8 (Figs. 10 and S11). This emphasizes the overestimation of TROPOMI NO_2 VCDs with the baseline simulation. The monthly NRMSE is 1.21 (Fig. 10). We have found that the baseline simulation is moderately correlated with the monthly average TROPOMI (R = 0.79).

https://doi.org/10.5194/egusphere-2026-2309
Preprint. Discussion started: 20 May 2026

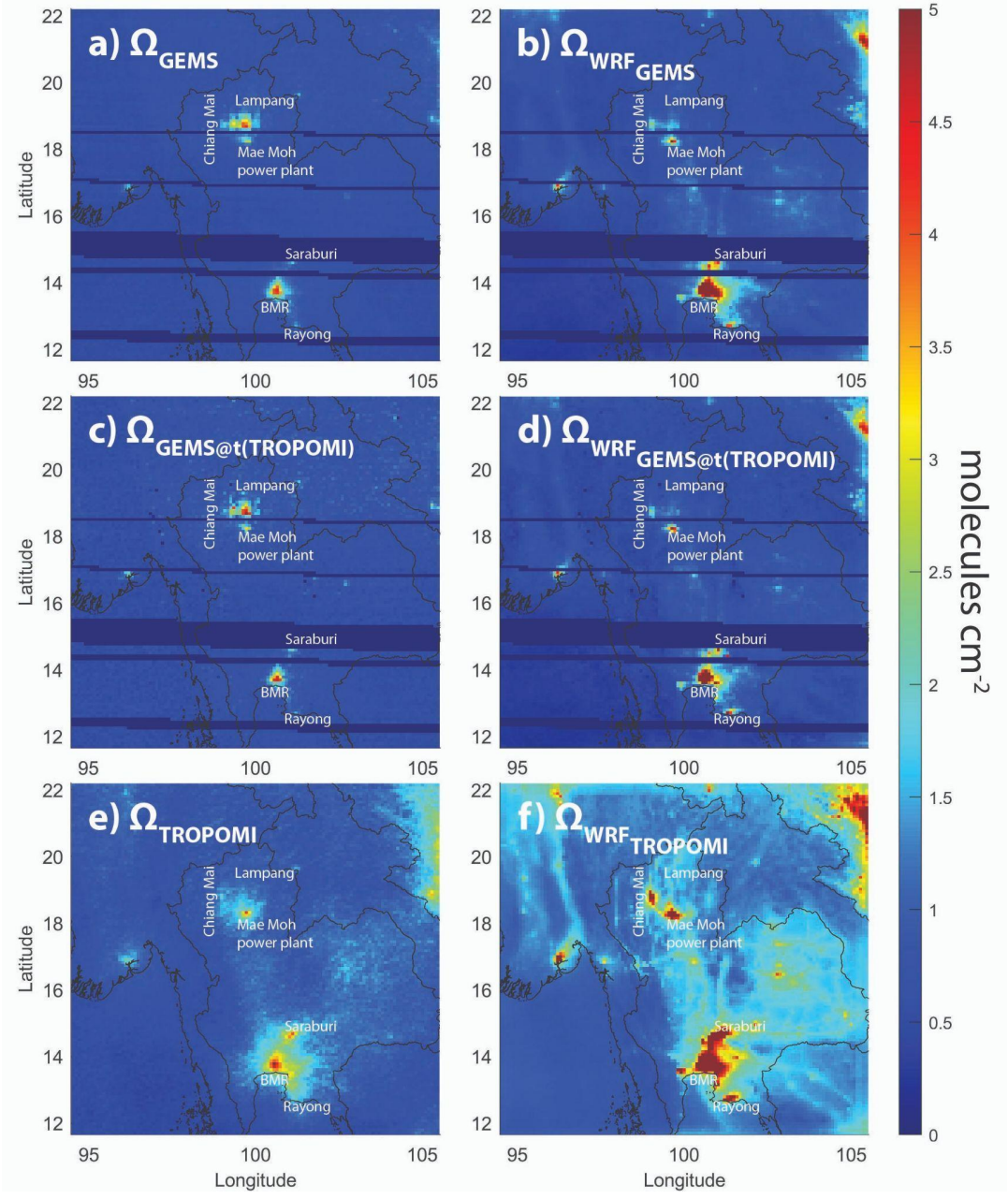

Figure 9: Monthly average tropospheric NO_2 VCD in September 2023 from: GEMS sampled at all available data (a), the baseline simulation applying GEMS averaging kernel sampled at GEMS scanning times (b), GEMS sampled at the TROPOMI overpass time (c), the baseline simulation applying the GEMS averaging kernel sampled at the TROPOMI overpass time (d), TROPOMI (e), and the baseline simulation applying the TROPOMI averaging kernel sampled at TROPOMI overpass time (f).

https://doi.org/10.5194/egusphere-2026-2309
Preprint. Discussion started: 20 May 2026

The IFDMB with fixed diurnal update significantly reduces NMB and NRMSE for TROPOMI, except in North Thailand. The NMB drops by roughly 25% relative to the baseline simulation, and NRMSE also declines by about 29% (Fig. 10). Because the baseline simulation overpredicts NO_2 in nearly all locations, the emission reductions from the IFDMB with fixed diurnal update lead to a closer match with TROPOMI across most of Thailand. For example, in the Bangkok Metropolitan Region and East Thailand, the IFDMB with fixed diurnal update significantly improves the NMB and NRMSE, while moderately reducing NMB and NRMSE in Central and Northeast Thailand (Figs. 10 and S11). In these areas, the NO_2 VCD from transportation and residential sectors is decreased, aligning better with the TROPOMI levels.

In contrast, the IFDMB with fixed diurnal update worsens the agreement with TROPOMI in North Thailand by increasing the NMB and NRMSE. This degradation is primarily due to the discrepancy between GEMS and TROPOMI NO_2 observations (Figs. 9c and 9e). While TROPOMI shows relatively low NO_2 VCDs in North Thailand compared to the Bangkok Metropolitan Region, GEMS has high NO_2 VCDs in the North. Moreover, the baseline simulation already overestimates NO_2 VCDs in North Thailand relative to TROPOMI (Fig. 10a). As a result, the IFDMB—driven by GEMS—further increases NOx emissions in the North, exacerbating the overestimation when compared to TROPOMI (Fig. 10b). This leads to a noticeable decline in the overall WRF-Chem–TROPOMI correlation, dropping to $R \approx 0.61$ (Fig. 10b). However, in the Bangkok Metropolitan Region, the update slightly improves the agreement, with monthly correlation coefficients increasing from 0.90 to 0.93 (Table S2).

The daylight diurnal and temporal average updates exhibit spatial trends similar to the fixed diurnal update, with improvements in most regions but degradation in North Thailand (Figs. 10 and S11). Across all grid cells, these two schemes do not yield net improvements in overall NMB and NRMSE (Fig. 10). The daylight diurnal update slightly increases NMB by 5% and reduces NRMSE by 2% relative to the baseline simulation. In contrast, the temporal average update increases NMB and NRMSE by 31% and 17%, respectively. The apparent deterioration in national-scale performance primarily stems from the mismatch between GEMS and TROPOMI in North Thailand.

To isolate this effect, we evaluate model performance in the Bangkok Metropolitan Region, where GEMS and TROPOMI show strong consistency (Table S2). In this region, the daylight diurnal update reduces NMB and NRMSE by 54% and 36%, respectively, compared with the baseline simulation (Table S2). The temporal average update yields even larger improvements, reducing NMB by 81% and NRMSE by 57% (Table S2). However, this update scheme performs the poorest in North Thailand. The temporal average update shows stronger emission adjustment near TROPOMI overpass time (09:00 - 11:00) compared to the daylight diurnal update. This leads to more impact on the model performance with TROPOMI.

Overall, the IFDMB with all three update schemes reduce the model bias and error in areas such as the Bangkok Metropolitan Region, Saraburi, and Rayong industrial estates. This is because TROPOMI's spatial pattern resembles GEMS, with high NO_2 VCDs over the Bangkok

https://doi.org/10.5194/egusphere-2026-2309
Preprint. Discussion started: 20 May 2026

Metropolitan Region and moderate VCDs over the Saraburi and Rayong industrial estates. However, improving model performance in North Thailand remains a challenge because GEMS and TROPOMI exhibit substantial differences in NO_2 VCDs over this region. TROPOMI NO_2 VCDs in North Thailand align more closely with the baseline simulation, having a strong signal from the Mae Moh power plant that is higher than the surrounding urban areas. In contrast, GEMS presents the highest NO_2 VCDs over the Lampang urban area instead. The inconsistency between GEMS and TROPOMI in North Thailand is a crucial finding.

Our analysis indicates that the GEMS–TROPOMI discrepancy primarily arises from uncertainties in the prior model profile used by the GEMS retrieval algorithm. TROPOMI version 2 uses the TM5-MP global model with the MACCity emission inventory for its retrieval algorithm (Douros et al., 2023; Williams et al., 2017). GEMS version 3 employs the GEOS-Chem model with the ASIA-AQv3 emission inventory as its prior input for NO_2 retrievals. Our analysis shows that the ASIA-AQv3 inventory reports anomalously high NO_x emissions in the Lampang region compared to other inventories (Fig. S6). This high NO_x emission likely causes GEMS to overestimate NO_2 VCDs over Lampang which is not observed by TROPOMI and the baseline simulation. The high NO_x emissions from ASIA-AQv3 also result in significantly larger retrieval errors in the Lampang area (Fig. 2). Supporting this interpretation, GEMS NO_2 using the Direct Vertical Column Fitting (DVCF) algorithm from Yang et al. (2023) yields much lower NO_2 VCDs over Lampang, in line with the TROPOMI observations. Notably, the GEMS version 3 data used in this study do agree well with TROPOMI over the Bangkok Metropolitan Region, Saraburi, and Rayong. Detailed comparisons are provided in Sects. S2 and S3.

These differences between satellite products highlight the importance of bias correction, calibration, and cross-validation for satellite-based NO_2 measurements. For example, Kim et al. (2023a) also find that both GEMS and TROPOMI underestimate NO_2 VCDs compared to Pandora measurements in Seosan, South Korea, with GEMS exhibiting a greater degree of underestimation than TROPOMI. The fact that GEMS and TROPOMI can yield markedly different NO_2 (as seen in Thailand) underscores the need to calibrate and validate these satellite retrievals using independent observations in Thailand. However, achieving robust calibration in Thailand is challenging due to the scarcity of ground-based measurements. In 2023, only a single Pandora spectrometer was operational in Bangkok. Data from this instrument exhibit substantial uncertainty during the Thai winter season (October–January) (Kanchanachat, 2026), and there is no cross-validation by other instruments. Furthermore, compared to Korea, China, and Japan, the Bangkok Pandora site reports significantly lower NO_2 VCDs relative to GEMS (Jung et al., 2025). Consequently, we exclude its observations from our analysis. We recommend leveraging data from the ASIA-AQ field campaign to improve the accuracy and consistency of satellite NO_2 assessments in Thailand. Even though this field campaign is limited to the Bangkok and Chiang Mai areas and spans only a short time period, it provides useful information to resolve the biases in the satellite products.

https://doi.org/10.5194/egusphere-2026-2309
Preprint. Discussion started: 20 May 2026

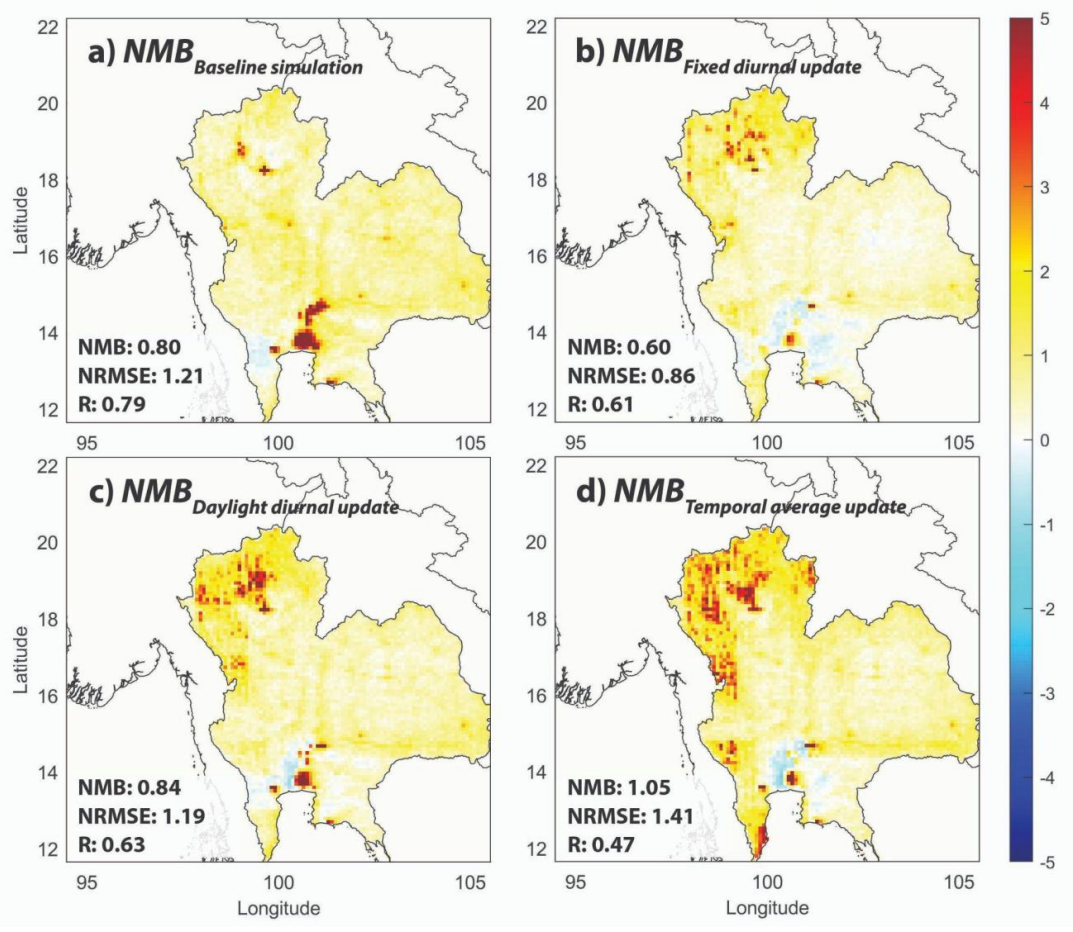

Figure 10: NMB of NO_2 VCD between WRF-Chem and TROPOMI of IFDMB for September 2023 using (a) prior emissions, and emissions updated by (b) fixed diurnal, (c) daylight diurnal, and (d) temporal average update schemes. Monthly statistical evaluations averaged across all grid cells in Thailand are provided for each simulation.

3.6 Comparison with data from PCD stations

Hourly observations from PCD stations are used to evaluate how different emission update schemes affect the simulated diurnal variability of NO_x. As the GEMS hourly scanning times occur between 08:00 and 15:00 Thailand local time, model–observation comparisons are limited to daylight hours. We restrict the comparison to 08:00 - 15:00 local time period to ensure a fair evaluation, as only the fixed diurnal scheme adjusts emissions outside this period, while the others revert to the prior emissions. The PCD stations are mostly located in Central and Northeast Thailand, and the Bangkok Metropolitan Region (Fig. S8). The baseline simulation systematically underestimates monthly average NO_x mixing ratios by 10-15 ppbv at 14 roadside PCD sites throughout the day and underestimates daytime NO_x by 3 ppbv or less at six non-

https://doi.org/10.5194/egusphere-2026-2309
Preprint. Discussion started: 20 May 2026

roadside PCD sites (Fig. S12). The IFDMB with GEMS-based top-down emission adjustment exacerbates the underestimation of NO_x mixing ratios at roadside PCD stations (Fig. S12), although it provides the same magnitude of concentration for non-roadside PCD stations. All inversion schemes lead to an increase in bias and error at roadside stations. These discrepancies arise primarily from differences in spatial resolution between the GEMS (~3.5 × 8 km^2), WRF-Chem (9 × 9 km^2), and PCD stations (point-scale), as well as strong local contributions of transportation emissions at the PCD sites. Moreover, both GEMS observations and WRF-Chem simulations are regridded to 81 × 81 km^2 for the mass balance calculation in this study to reduce smearing errors associated with horizontal transport. However, this introduces resolution errors by averaging over spatially heterogeneous emission sources. This grid-averaged value is heavily influenced by regional NO_2 pollution and is therefore much lower than the NO_2 mixing ratio from local hotspots, such as a busy roadway, that may occupy only a small fraction of that grid cell. Consequently, we do not focus on reproducing absolute NO_x mixing ratios in this study but instead assess hangs and improvements in diurnal patterns as shown in NO_x concentrations normalized by their monthly average value (Fig. 11).

Observed NO_x mixing ratios typically peak near 08:00, during the morning rush hour, whereas the baseline simulation and WRF-Chem simulations using posterior emissions have an earlier peak between 06:00 and 07:00. Furthermore, the model has higher NO_x levels at night, while observations have high NO_x during the day. This discrepancy indicates that the diurnal profile from Thongsame et al. (2024) used in the baseline simulation does not fully capture the real-world traffic patterns for NO_x. In particular, the default diurnal profile fails to reproduce the morning traffic peak and instead shows a high level of NO_x during nighttime. The fixed diurnal update scheme does not improve the temporal correlation between modeled and observed NO_x mixing ratios at roadside or non-roadside stations (Fig. 14). As this update scheme does not alter the shape of the diurnal profile, the simulated NO_x peak continues to occur at night, leaving the morning underestimation unresolved. The daylight diurnal and temporal average updates also show limited improvement in diurnal variability (Fig. 14). At roadside stations, both produce afternoon NO_x diurnal variability closer to that of the PCD data but fail to reproduce the morning peak. At non-roadside stations, both schemes capture similar morning diurnal variability yet diverge in the afternoon. The temporal average update yields a slight mid-day dip, whereas the daylight diurnal update produces a modest increase (Fig. 14). The PCD data exhibit a small increase around 14:00 and a drop by 15:00, which is more consistent with the daylight diurnal update. Overall, the GEMS-based diurnal variability does not capture the observed morning rush-hour but slightly improves afternoon diurnal variability. However, using the GEMS satellite to only update the diurnal variability introduces an unrealistic diurnal profile in the model – an abrupt increase and drop in the NO_x emissions profile (Fig. 9). We recommend implementing a smoothing technique in future work to mitigate such discontinuities. In summary, while the fixed diurnal update does not improve model–observation agreement due to its unchanged emission profile, the daylight diurnal and temporal average updates offer some potential for spatially resolved diurnal refinements. However, the lack of satellite observations during critical rush-hour periods (early morning and evening) limits their effectiveness. Although GEMS-based updates alone do not substantially improve NO_x simulations at PCD stations due to resolution and timing

https://doi.org/10.5194/egusphere-2026-2309
Preprint. Discussion started: 20 May 2026

mismatches, the satellite provides valuable information for refining regionally specific diurnal patterns, which could enhance WRF-Chem performance in future studies.

Our findings also underscore the tradeoffs in the application of mass balance methods. The IFDMB approach, when applied at the 81 × 81 km^2 resolution, offers computational efficiency and is well-suited for adjusting regional-scale emissions over long temporal periods. However, its coarse spatial resolution limits its ability to capture fine-scale urban variability and accurately constrain emissions from local sources such as traffic. In contrast, other inversion techniques—such as 4D-Var or ensemble Kalman filter (EnKF) methods—coupled with high-resolution models, would be more effective for resolving local emissions. However, these approaches are computationally expensive and may not be feasible for long-term simulation. Therefore, the IFDMB with GEMS data provides practical and efficient adjustments to regional NO_x emissions in Thailand.

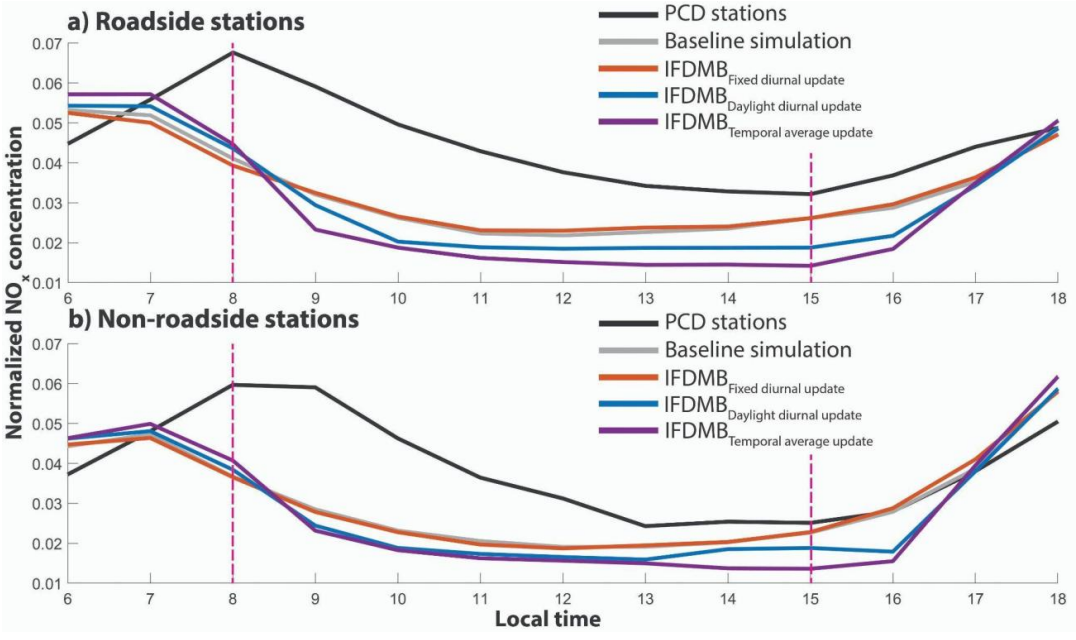

Figure 11: The daytime diurnal variability of normalized NO_x concentrations from PCD stations (black) and WRF-Chem: the baseline simulation (gray), IFDMB with fixed diurnal update (orange), IFDMB with daylight diurnal update (blue), and IFDMB with temporal average update (purple). PCD stations are classified into roadside stations (a) and non-roadside stations (b). The pink line is the GEMS scanning time in Thailand from 08:00 - 15:00 local time.

3.7 Inversion approaches

This section provides an evaluation of the performance and inherent trade-offs of the different update schemes used in our study. The IFDMB method is a practical advancement of the mass

https://doi.org/10.5194/egusphere-2026-2309
Preprint. Discussion started: 20 May 2026

balance approach for emission adjustment by integrating satellite and prior information. In our study, regularization parameters C_1 and C_2 are introduced to balance constraints between the prior emissions and GEMS. These parameters control the trade-off between overfitting and underfitting to the satellite data. For example, the discrepancy between GEMS and TROPOMI in North Thailand indicates high uncertainty in the satellite observations. In this region, a higher C_1 value, which affects the prediction error term, allows IFDMB to place less weight on the GEMS data, reducing the risk of over-adjustment in areas with more uncertain observations. Although our study does not fully evaluate the sensitivity of IFDMB to C_1 and C_2, preliminary tests with varying parameter values are presented in Sect. S1.

We find that with C_1 = 1 × 10^{14}, IFDMB can partially accommodate the uncertainty in the GEMS data due to ASIA-AQv3 inventory used for the GEMS retrieval. Our IFDMB still leads to increased bias and error for WRF-Chem in North Thailand when compared with TROPOMI, particularly for the daylight diurnal and temporal average update schemes. These schemes are more uncertain than the fixed diurnal update because of fewer available data points in each update. The C_2 parameter, which affects the emissions error term, helps prevent IFDMB from excessively adjusting small emissions, but our results indicate that C_1 has a stronger influence on IFDMB performance than C_2. The overall performance of IFDMB also depends on the relative uncertainties from GEMS and the prior emissions. In this study, we apply a fixed uncertainty of 50% to the prior emissions, which may not reflect the true variability in real-world conditions. Additionally, the GEMS error is lower than the error reported in TROPOMI. Therefore, future work should focus on developing more accurate, region-specific estimates of both satellite and prior emission uncertainties to further improve IFDMB performance and reliability.

For the update schemes, while all three schemes for IFDMB offer improvements over the prior simulation when evaluated against GEMS data, the analysis reveals that no single scheme is consistently the best. Each method has trade-offs in the treatment of diurnal variability, which leads to varied performance. The fixed diurnal update, which applies a uniform monthly-averaged correction factor to emissions at all hours, produces the most substantial improvements against GEMS observations. However, this method could not correct the diurnal variability of emissions. The ground-based PCD data clearly show that the baseline simulation misrepresents the diurnal cycle, with the model peaking at night instead of during morning and evening rush hours. The high NO_x concentration during the nighttime from the model is likely due to the low planetary boundary layer at that time (Thongsame et al., 2024). The fixed diurnal update simply scales down the incorrect diurnal profile, without improving the diurnal variability. The daylight diurnal and temporal average updates are designed to address diurnal issues by incorporating hourly GEMS data. These schemes only adjust emissions during daylight hours, resulting in more modest improvements in GEMS agreement. Their key weakness, however, is the introduction of an unrealistic diurnal profile. Because the algorithms have no observational constraints outside the GEMS timing window, they revert to the prior profile at night. This is due to the limitations of our update schemes. This limitation reflects the challenges of refining emissions outside the GEMS coverage period, as no UV/Vis satellite observations are available at night. Future research should consider integrating additional datasets—such as from the

https://doi.org/10.5194/egusphere-2026-2309
Preprint. Discussion started: 20 May 2026

recent ASIA-AQ field campaign data, Pandora spectrometer measurements, and PCD stations—with satellite observations to develop accurate diurnal profiles. Nevertheless, GEMS provides valuable information for constraining daylight diurnal variability across different regions of Thailand.

3.8 Comparison with previous studies

We compare our results with another study using GEMS to adjust regional emissions. Our baseline simulation shows consistent results with Park et al. (2024) when comparing monthly average NO_2 VCDs with GEMS data. Specifically, in our September 2023 simulation, the baseline simulation overestimates NO_2 VCDs across most of Thailand, except in the North. Similarly, using the CMAQ model for March–April 2022, Park et al. (2024) report an overestimation of NO_2 VCD compared to GEMS across all regions of Thailand, including the North. The key difference in the North is due to the dominant emission sources during the two study periods. In Park et al. (2024), the simulation period is during the haze season, when biomass burning emissions mainly contribute to NO_x in North Thailand during March–April (Lalitaporn, 2017; Oo et al., 2021). In contrast, our study period in September 2023 corresponds to the non-haze season, when biomass burning activity is minimal. Therefore, the underestimation in North Thailand, in our case, is likely attributable to anthropogenic emission inventories rather than biomass burning. Additionally, Park et al. (2024) use GEMS version 2 for emission adjustment, while our study utilizes GEMS version 3, which may also contribute to differences.

Regarding top-down emission updates, our IFDMB produces similar regional trends to Park et al. (2024) across all update schemes. In both studies, posterior NO_x emissions decrease in the Bangkok Metropolitan Region, Central, and Northeast Thailand. However, our study shows an increase in posterior NO_x emissions in North Thailand, while Park et al. (2024) report a decrease in this region. This contrast again likely reflects seasonal differences in emission sources—anthropogenic in our case, biomass burning in theirs.

Our analysis also shows that the daylight diurnal and temporal average update schemes produce higher simulation errors in the morning hours when evaluated against GEMS, compared to midday periods. This pattern arises because these update schemes modify emissions only during daylight hours while leaving nighttime emissions unchanged. Although NO_2 is a short-lived species, it still can have a multi-hour lifetime, meaning that emissions from previous hours influence concentrations at any given time. Consequently, unchanged nighttime emissions can impact early morning NO_2 concentrations. Furthermore, as noted in recent work (Lange et al., 2024; Park et al., 2024), GEMS observations in the early morning and late afternoon are subject to greater uncertainty due to unfavorable viewing geometries, often leading to underestimation of NO_2 columns. This observational bias further complicates the evaluation of morning model performance when using GEMS data alone. In the future, we plan to integrate other observations, which provide nighttime data, for these update schemes. As our study is one of the first applications of GEMS geostationary data to update local emissions specifically focused on Thailand, we have not yet applied other instruments to infer nighttime anthropogenic activities such as thermal infrared (TIR) instruments or VIIRS night light products.

https://doi.org/10.5194/egusphere-2026-2309
Preprint. Discussion started: 20 May 2026

4. Conclusion

This study applies high-temporal-resolution GEMS satellite data to update anthropogenic NO_x emissions over Thailand during September 2023 to improve the air quality modeling and access diurnal variability of emissions. We compare WRF-Chem simulations using posterior emissions with observations from both the satellite and surface PCD stations to highlight the strengths and limitations of the IFDMB method using GEMS. We find that the baseline simulation from CAMS-GLOB-ANT v5.3 significantly overestimates tropospheric NO_2 VCDs across Thailand in comparison to both GEMS and TROPOMI, except in North Thailand where GEMS indicates this inventory is an underestimation. By applying the IFDMB inversion technique, the fixed diurnal update increases NO_x emission by about 20 mol km^{-2} hr^{-1} in North and West Thailand while decreasing them by about 30 mol km^{-2} hr^{-1} across most other regions. In contrast, the daylight diurnal and temporal average updates produce generally smaller adjustments. WRF-Chem simulations using posterior emissions show improved agreement with TROPOMI in most regions, especially the Bangkok Metropolitan Region. In this area, the fixed diurnal and temporal average updates achieve NMB reductions of 83% and 81%, and NRMSE reductions of 76% and 61%, respectively. The daylight diurnal update reduces NMB by 54% and NRMSE by 39%. However, the improvement in North Thailand is limited due to the discrepancy between GEMS and TROPOMI data in this area. Evaluation against PCD stations shows that the baseline simulation underestimates NO_x mixing ratios by 10–15 ppbv at roadside site. WRF-Chem using posterior emissions further exacerbates this underestimation at roadside PCD stations. This is attributed to strong differences in spatial resolution combined with the short lifetime of NO_x. The roadside PCD stations are mainly influenced by local transportation emissions, whereas GEMS captures broader urban and industrial emissions. Despite this limitation, GEMS demonstrates the potential to constrain the area-specific daytime diurnal variability of NO_x emissions, allowing diurnal emission profiles to be updated for each region rather than applying a uniform diurnal profile. This leads the model to be more accurate and reflects real-world emission patterns.

Our results are broadly consistent with previous study using GEMS data to constrain NO_x emissions over Southeast Asia during the haze season (March–April 2022). Both simulations overestimate NO_2 VCDs relative to GEMS across most regions which results in NO_x emission reductions across Thailand. However, our IFDMB approaches increase the NO_x emissions in North Thailand during October 2023 whereas previous study decreases the emissions. This key divergence is mainly due to the high biomass burning emission in haze season and the differences between GEMS versions. Moreover, our study highlights the limitations of mass balance method using GEMS observation for refining NO_x emissions in Thailand. The coarsening of GEMS and WRF-Chem data to 81 x 81 km^2 for mass balance method reduces smearing errors, but introduces resolution errors that prevent accurate representation of local traffic emission. A further limitation is the discrepancy between GEMS and TROPOMI NO_2 in North Thailand, which is attributed to the a priori emission inventory used in the GEMS retrieval algorithm. This emphasizes the calibration and bias correction for satellite data in Thailand in the future.

In summary, this study demonstrates both the value and limitations of GEMS observations for refining NO_x emissions in Thailand. GEMS provides valuable insights into the spatial distribution

https://doi.org/10.5194/egusphere-2026-2309
Preprint. Discussion started: 20 May 2026

and daylight diurnal variability of NO_x across the region. By integrating GEMS data with mass balance methods, we improve the performance of NO_x simulations using WRF-Chem, particularly in the Bangkok Metropolitan Region, which showed substantial improvement when compared to TROPOMI observations. These results underscore the benefits of geostationary satellites such as GEMS for near-real-time emission constraint. However, limitations related to satellite retrieval uncertainty, spatial resolution, and local emission representation remain challenges Thailand. For future work, we recommend combining GEMS observations with complementary datasets—such as PCD stations, LEO satellite, and data from the recent ASIA-AQ field campaign—to enhance data assimilation and reduce potential biases in GEMS retrievals.

Code and data availability

The source code for WRF-Chem version 4.2.2 (Skamarock et al., 2019) is available at https://github.com/wrf-model/WRF. The model configuration follows Thongsame et al. (2024), incorporating biomass burning emissions from FINN2.5 (Wiedinmyer et al., 2023) and anthropogenic emissions from CAMS-GLOB-ANT v5.3 (Granier et al., 2019).

Observation data from PCD stations can be accessed at http://air4thai.pcd.go.th/webV3/. The GEMS data are available at https://nesc.nier.go.kr/en/html/index.do. The information of TROPOMI data can be found at https://www.tropomi.eu/.

Author contributions. WT and DKH designed the experiments, and WT carried them out. RK, MB, and GP provide resources and supervision. All authors edited the manuscript.

Competing interests. The contact author has declared that none of the authors has any competing interests.

Disclaimer. Copernicus Publications remains neutral with regard to jurisdictional claims made in the text, published maps, institutional affiliations, or any other geographical representation in this paper. While Copernicus Publications makes every effort to include appropriate place names, the final responsibility lies with the authors. Views expressed in the text are those of the authors and do not necessarily reflect the views of the publisher.

Acknowledgements. WT is supported by the Development and Promotion of Science and Technology Talents Project (DPST) fellowship, Royal Thai government. WT and DKH recognize support from NASA 80NSSC22K1047. RK, MB, and GP are supported by the NSF National Center for Atmospheric Research (NCAR), which is a major facility sponsored by the U.S. National Science Foundation under Cooperative Agreement No. 1852977.

We acknowledge use of the WRF-Chem preprocessor tools {mozbc, fire_emiss, etc.} provided by the Atmospheric Chemistry Observations and Modeling Lab (ACOM) of NCAR. We would like to acknowledge high-performance computing support from Derecho (https://doi.org/10.5065/qx9a-pg09) provided by NCAR's Computational and Information Systems Laboratory, sponsored by the National Science Foundation.

https://doi.org/10.5194/egusphere-2026-2309
Preprint. Discussion started: 20 May 2026

References

Adams, P. J., Seinfeld, J. H., Koch, D., Mickley, L., and Jacob, D.: General circulation model assessment of direct radiative forcing by the sulfate-nitrate-ammonium-water inorganic aerosol system, J. Geophys. Res. Atmospheres, 106, 1097–1111, https://doi.org/10.1029/2000JD900512, 2001.

Boersma, K. F., Jacob, D. J., Bucsela, E. J., Perring, A. E., Dirksen, R., Van Der A, R. J., Yantosca, R. M., Park, R. J., Wenig, M. O., and Bertram, T. H.: Validation of OMI tropospheric NO2 observations during INTEX-B and application to constrain NOxNOx emissions over the eastern United States and Mexico, Atmos. Environ., 42, 4480–4497, https://doi.org/10.1016/j.atmosenv.2008.02.004, 2008.

Chen, D., Li, Q., Stutz, J., Mao, Y., Zhang, L., Pikelnaya, O., Tsai, J. Y., Haman, C., Lefer, B., Rappenglück, B., Alvarez, S. L., Neuman, J. A., Flynn, J., Roberts, J. M., Nowak, J. B., De Gouw, J., Holloway, J., Wagner, N. L., Veres, P., Brown, S. S., Ryerson, T. B., Warneke, C., and Pollack, I. B.: WRF-chem simulation of NOx and O3 in the L.A. basin during CalNex-2010, Atmos. Environ., 81, 421–432, https://doi.org/10.1016/j.atmosenv.2013.08.064, 2013.

Choi, W. J.: Introducing the geostationary environment monitoring spectrometer, J. Appl. Remote Sens., 12, 1, https://doi.org/10.1117/1.JRS.12.044005, 2018.

Cooper, M., Martin, R. V., Padmanabhan, A., and Henze, D. K.: Comparing mass balance and adjoint methods for inverse modeling of nitrogen dioxide columns for global nitrogen oxide emissions, J. Geophys. Res. Atmospheres, 122, 4718–4734, https://doi.org/10.1002/2016JD025985, 2017.

Cooper, M. J., Martin, R. V., Henze, D. K., and Jones, D. B. A.: Effects of a priori profile shape assumptions on comparisons between satellite NO_2 columns and model simulations, Atmospheric Chem. Phys., 20, 7231–7241, https://doi.org/10.5194/acp-20-7231-2020, 2020.

Crippa, M., Guizzardi, D., Butler, T., Keating, T., Wu, R., Kaminski, J., Kuenen, J., Kurokawa, J., Chatani, S., Morikawa, T., Pouliot, G., Racine, J., Moran, M. D., Klimont, Z., Manseau, P. M., Mashayekhi, R., Henderson, B. H., Smith, S. J., Suchyta, H., Muntean, M., Solazzo, E., Banja, M., Schaaf, E., Pagani, F., Woo, J.-H., Kim, J., Monforti-Ferrario, F., Pisoni, E., Zhang, J., Niemi, D., Sassi, M., Ansari, T., and Foley, K.: The HTAP_v3 emission mosaic: merging regional and global monthly emissions (2000–2018) to support air quality modelling and policies, Earth Syst. Sci. Data, 15, 2667–2694, https://doi.org/10.5194/essd-15-2667-2023, 2023.

De Foy, B., Wilkins, J. L., Lu, Z., Streets, D. G., and Duncan, B. N.: Model evaluation of methods for estimating surface emissions and chemical lifetimes from satellite data, Atmos. Environ., 98, 66–77, https://doi.org/10.1016/j.atmosenv.2014.08.051, 2014.

Delmas, R., Serça, D., and Jambert, C.: Global inventory of NOx sources, Nutr. Cycl. Agroecosystems, 48, 51–60, https://doi.org/10.1023/A:1009793806086, 1997.

https://doi.org/10.5194/egusphere-2026-2309
Preprint. Discussion started: 20 May 2026

930 Ding, J., Miyazaki, K., Van Der A, R. J., Mijling, B., Kurokawa, J., Cho, S., Janssens-Maenhout,
931 G., Zhang, Q., Liu, F., and Levelt, P. F.: Intercomparison of NOx emission inventories over east
932 asia, Atmospheric Chem. Phys., 17, 10125–10141, https://doi.org/10.5194/acp-17-10125-2017,
933 2017.

934 Douros, J., Eskes, H., Van Geffen, J., Boersma, K. F., Compernolle, S., Pinardi, G.,
935 Blechschmidt, A.-M., Peuch, V.-H., Colette, A., and Veefkind, P.: Comparing Sentinel-5P
936 TROPOMI NO_2 column observations with the CAMS regional air quality ensemble, Geosci.
937 Model Dev., 16, 509–534, https://doi.org/10.5194/gmd-16-509-2023, 2023.

938 Drinkwater, A., Palmer, P. I., Feng, L., Arnold, T., Lan, X., Michel, S. E., Parker, R., and Boesch,
939 H.: Atmospheric data support a multi-decadal shift in the global methane budget towards natural
940 tropical emissions, Atmospheric Chem. Phys., 23, 8429–8452, https://doi.org/10.5194/acp-23-
941 8429-2023, 2023.

942 Emmons, L. K., Walters, S., Hess, P. G., Guenther, A., Kinnison, D., Laepple, T., Orlando, J.,
943 Tie, X., Tyndall, G., Wiedinmyer, C., Baughcum, S. L., and Kloster, S.: Description and
944 evaluation of the model for ozone and related chemical tracers, version 4 (MOZART-4), Geosci
945 Model Dev, 2010.

946 Eum, K.-D., Honda, T. J., Wang, B., Kazemiparkouhi, F., Manjourides, J., Pun, V. C., Pavlu, V.,
947 and Suh, H.: Long-term nitrogen dioxide exposure and cause-specific mortality in the U.S.
948 medicare population, Environ. Res., 207, 112154, https://doi.org/10.1016/j.envres.2021.112154,
949 2022.

950 Fast, J. D., Gustafson, W. I., Easter, R. C., Zaveri, R. A., Barnard, J. C., Chapman, E. G., Grell,
951 G. A., and Peckham, S. E.: Evolution of ozone, particulates, and aerosol direct radiative forcing
952 in the vicinity of houston using a fully coupled meteorology-chemistry-aerosol model, J.
953 Geophys. Res. Atmospheres, 111, 2005JD006721, https://doi.org/10.1029/2005JD006721,
954 2006.

955 Ghude, S. D., Pfister, G. G., Jena, C., Van Der A, R. J., Emmons, L. K., and Kumar, R.: Satellite
956 constraints of nitrogen oxide (NO_x) emissions from India based on OMI observations and WRF-
957 Chem simulations, Geophys. Res. Lett., 40, 423–428, https://doi.org/10.1002/grl.50065, 2013.

958 Granier, C., Darras, S., Denier van der Gon, H., Doubalova, J., Elguindi, N., Galle, B., Gauss,
959 M., Guevara, M., Jalkanen, J.-P., Kuenen, J., Liousse, C., Quack, B., Simpson, D., and
960 Sindelarova, K.: The copernicus atmosphere monitoring service global and regional emissions
961 (april 2019 version), https://doi.org/10.24380/D0BN-KX16, 2019.

962 Grell, G. A., Peckham, S. E., Schmitz, R., McKeen, S. A., Frost, G., Skamarock, W. C., and
963 Eder, B.: Fully coupled “online” chemistry within the WRF model, Atmos. Environ., 39, 6957–
964 6975, https://doi.org/10.1016/j.atmosenv.2005.04.027, 2005.

965 Guenther, A., Karl, T., Harley, P., Wiedinmyer, C., Palmer, P. I., and Geron, C.: Estimates of
966 global terrestrial isoprene emissions using MEGAN (model of emissions of gases and aerosols
967 from nature), Atmos Chem Phys, 2006.

https://doi.org/10.5194/egusphere-2026-2309
Preprint. Discussion started: 20 May 2026

968 Horner, R. P., Marais, E. A., Wei, N., Ryan, R. G., and Shah, V.: Vertical profiles of global
969 tropospheric nitrogen dioxide (NO_2) obtained by cloud slicing the TROPOspheric monitoring
970 instrument (TROPOMI), Atmospheric Chem. Phys., 24, 13047–13064,
971 https://doi.org/10.5194/acp-24-13047-2024, 2024.

972 Jena, C., Ghude, S. D., Beig, G., Chate, D. M., Kumar, R., Pfister, G. G., Lal, D. M., Surendran,
973 D. E., Fadnavis, S., and Van Der A, R. J.: Inter-comparison of different NOX emission
974 inventories and associated variation in simulated surface ozone in Indian region, Atmos.
975 Environ., 117, 61–73, https://doi.org/10.1016/j.atmosenv.2015.06.057, 2015.

976 Jeong, U. and Hong, H.: Assessment of tropospheric concentrations of NO2 from the
977 TROPOMI/sentinel-5 precursor for the estimation of long-term exposure to surface NO2 over
978 south korea, Remote Sens., 13, 1877, https://doi.org/10.3390/rs13101877, 2021.

979 Ji, X., Han, M., Yun, Y., Li, G., and Sang, N.: Acute nitrogen dioxide (NO2) exposure enhances
980 airway inflammation via modulating Th1/Th2 differentiation and activating JAK-STAT pathway,
981 Chemosphere, 120, 722–728, https://doi.org/10.1016/j.chemosphere.2014.10.039, 2015.

982 Judd, L. M., Al-Saadi, J. A., Szykman, J. J., Valin, L. C., Janz, S. J., Kowalewski, M. G., Eskes,
983 H. J., Veefkind, J. P., Cede, A., Mueller, M., Gebetsberger, M., Swap, R., Pierce, R. B., Nowlan,
984 C. R., Abad, G. G., Nehrir, A., and Williams, D.: Evaluating sentinel-5P TROPOMI tropospheric
985 NO_2 column densities with airborne and pandora spectrometers near new york city and long
986 island sound, Atmospheric Meas. Tech., 13, 6113–6140, https://doi.org/10.5194/amt-13-6113-
987 2020, 2020.

988 Jung, J., Choi, Y., Souri, A. H., Mousavinezhad, S., Sayeed, A., and Lee, K.: The impact of
989 springtime-transported air pollutants on local air quality with satellite-constrained NO_x emission
990 adjustments over east asia, J. Geophys. Res. Atmospheres, 127, e2021JD035251,
991 https://doi.org/10.1029/2021JD035251, 2022.

992 Jung, Y., Park, J., Hong, H., Lee, H., and Jeong, U.: Evaluation of GEMS NO2 Retrieval
993 Algorithm Version 2.0 and 3.0 Using TROPOMI and Pandora Observations, Korean J. Remote
994 Sens., 41, 803–811, https://doi.org/10.7780/kjrs.2025.41.5.8, 2025.

995 Kanchanachat, W.: Assessment of Pandora and S5P/TROPOMI observations for investigating
996 tropospheric NO2 vertical column densities in Thailand, Atmos. Environ., 367, 121738,
997 https://doi.org/10.1016/j.atmosenv.2025.121738, 2026.

998 Kim, J., Jeong, U., Ahn, M.-H., Kim, J. H., Park, R. J., Lee, H., Song, C. H., Choi, Y.-S., Lee, K.-
999 H., Yoo, J.-M., Jeong, M.-J., Park, S. K., Lee, K.-M., Song, C.-K., Kim, S.-W., Kim, Y. J., Kim,
1000 S.-W., Kim, M., Go, S., Liu, X., Chance, K., Chan Miller, C., Al-Saadi, J., Veihelmann, B.,
1001 Bhartia, P. K., Torres, O., Abad, G. G., Haffner, D. P., Ko, D. H., Lee, S. H., Woo, J.-H., Chong,
1002 H., Park, S. S., Nicks, D., Choi, W. J., Moon, K.-J., Cho, A., Yoon, J., Kim, S., Hong, H., Lee, K.,
1003 Lee, H., Lee, S., Choi, M., Veefkind, P., Levelt, P. F., Edwards, D. P., Kang, M., Eo, M., Bak, J.,
1004 Baek, K., Kwon, H.-A., Yang, J., Park, J., Han, K. M., Kim, B.-R., Shin, H.-W., Choi, H., Lee, E.,
1005 Chong, J., Cha, Y., Koo, J.-H., Irie, H., Hayashida, S., Kasai, Y., Kanaya, Y., Liu, C., Lin, J.,
1006 Crawford, J. H., Carmichael, G. R., Newchurch, M. J., Lefer, B. L., Herman, J. R., Swap, R. J.,

https://doi.org/10.5194/egusphere-2026-2309
Preprint. Discussion started: 20 May 2026

Lau, A. K. H., Kurosu, T. P., Jaross, G., Ahlers, B., Dobber, M., McElroy, C. T., and Choi, Y.: New era of air quality monitoring from space: geostationary environment monitoring spectrometer (GEMS), Bull. Am. Meteorol. Soc., 101, E1–E22, https://doi.org/10.1175/BAMS-D-18-0013.1, 2020.

Kim, K.-M., Kim, S.-W., Seo, S., Blake, D. R., Cho, S., Crawford, J. H., Emmons, L. K., Fried, A., Herman, J. R., Hong, J., Jung, J., Pfister, G. G., Weinheimer, A. J., Woo, J.-H., and Zhang, Q.: Sensitivity of the WRF-Chem v4.4 simulations of ozone and formaldehyde and their precursors to multiple bottom-up emission inventories over East Asia during the KORUS-AQ 2016 field campaign, Geosci. Model Dev., 17, 1931–1955, https://doi.org/10.5194/gmd-17-1931-2024, 2024.

Kim, S., Kim, D., Hong, H., Chang, L.-S., Lee, H., Kim, D.-R., Kim, D., Yu, J.-A., Lee, D., Jeong, U., Song, C.-K., Kim, S.-W., Park, S. S., Kim, J., Hanisco, T. F., Park, J., Choi, W., and Lee, K.: First-time comparison between NO $_2$ vertical columns from geostationary environmental monitoring spectrometer (GEMS) and pandora measurements, Atmospheric Meas. Tech., 16, 3959–3972, https://doi.org/10.5194/amt-16-3959-2023, 2023a.

Kim, S., Kim, D., Hong, H., Chang, L.-S., Lee, H., Kim, D.-R., Kim, D., Yu, J.-A., Lee, D., Jeong, U., Song, C.-K., Kim, S.-W., Park, S. S., Kim, J., Hanisco, T. F., Park, J., Choi, W., and Lee, K.: First-time comparison between NO_2 vertical columns from Geostationary Environmental Monitoring Spectrometer (GEMS) and Pandora measurements, Atmospheric Meas. Tech., 16, 3959–3972, https://doi.org/10.5194/amt-16-3959-2023, 2023b.

Knote, C., Hodzic, A., Jimenez, J. L., Volkamer, R., Orlando, J. J., Baidar, S., Brioude, J., Fast, J., Gentner, D. R., Goldstein, A. H., Hayes, P. L., Knighton, W. B., Oetjen, H., Setyan, A., Stark, H., Thalman, R., Tyndall, G., Washenfelder, R., Waxman, E., and Zhang, Q.: Simulation of semi-explicit mechanisms of SOA formation from glyoxal in aerosol in a 3-D model, Atmospheric Chem. Phys., 14, 6213–6239, https://doi.org/10.5194/acp-14-6213-2014, 2014.

Lalitaporn, P.: Temporal and spatial variability of tropospheric NO2 columns retrieved from OMI satellite data and comparison with ground based information in Thailand, Eng. Appl. Sci. Res., 44, 4, https://doi.org/10.14456/EASR.2017.35, 2017.

Lamsal, L. N., Martin, R. V., Padmanabhan, A., Van Donkelaar, A., Zhang, Q., Sioris, C. E., Chance, K., Kurosu, T. P., and Newchurch, M. J.: Application of satellite observations for timely updates to global anthropogenic NO $_x$ emission inventories: UPDATING NO $_x$ EMISSION INVENTORIES, Geophys. Res. Lett., 38, n/a-n/a, https://doi.org/10.1029/2010GL046476, 2011.

Lange, K., Richter, A., Bösch, T., Zilker, B., Latsch, M., Behrens, L. K., Okafor, C. M., Bösch, H., Burrows, J. P., Merlaud, A., Pinardi, G., Fayt, C., Friedrich, M. M., Dimitropoulou, E., Van Roozendael, M., Ziegler, S., Ripperger-Lukosiunaite, S., Kuhn, L., Lauster, B., Wagner, T., Hong, H., Kim, D., Chang, L.-S., Bae, K., Song, C.-K., and Lee, H.: Validation of GEMS tropospheric NO_2 columns and their diurnal variation with ground-based DOAS measurements, https://doi.org/10.5194/egusphere-2024-617, 28 March 2024.

https://doi.org/10.5194/egusphere-2026-2309
Preprint. Discussion started: 20 May 2026

1045 Li, C., Martin, R. V., Shephard, M. W., Cady-Pereira, K., Cooper, M. J., Kaiser, J., Lee, C. J.,
1046 Zhang, L., and Henze, D. K.: Assessing the iterative finite difference mass balance and 4D-var
1047 methods to derive ammonia emissions over north america using synthetic observations, J.
1048 Geophys. Res. Atmospheres, 124, 4222–4236, https://doi.org/10.1029/2018JD030183, 2019.

1049 Li, C., Martin, R. V., Cohen, R. C., Bindle, L., Zhang, D., Chatterjee, D., Weng, H., and Lin, J.:
1050 Variable effects of spatial resolution on modeling of nitrogen oxides, Atmospheric Chem. Phys.,
1051 23, 3031–3049, https://doi.org/10.5194/acp-23-3031-2023, 2023a.

1052 Li, Y., Xing, C., Peng, H., Song, Y., Zhang, C., Xue, J., Niu, X., and Liu, C.: Long-term
1053 observations of NO2 using GEMS in china: validations and regional transport, Sci. Total
1054 Environ., 904, 166762, https://doi.org/10.1016/j.scitotenv.2023.166762, 2023b.

1055 Lin, J.-T., McElroy, M. B., and Boersma, K. F.: Constraint of anthropogenic NO_x emissions in
1056 china from different sectors: a new methodology using multiple satellite retrievals, Atmospheric
1057 Chem. Phys., 10, 63–78, https://doi.org/10.5194/acp-10-63-2010, 2010.

1058 Liu, F., Zhang, Q., Van Der A, R. J., Zheng, B., Tong, D., Yan, L., Zheng, Y., and He, K.: Recent
1059 reduction in NO_x emissions over china: synthesis of satellite observations and emission
1060 inventories, Environ. Res. Lett., 11, 114002, https://doi.org/10.1088/1748-9326/11/11/114002,
1061 2016.

1062 Martin, R. V., Jacob, D. J., Chance, K., Kurosu, T. P., Palmer, P. I., and Evans, M. J.: Global
1063 inventory of nitrogen oxide emissions constrained by space-based observations of NO_2
1064 columns, J. Geophys. Res. Atmospheres, 108, 2003JD003453,
1065 https://doi.org/10.1029/2003JD003453, 2003.

1066 Miyazaki, K., Eskes, H., Sudo, K., Boersma, K. F., Bowman, K., and Kanaya, Y.: Decadal
1067 changes in global surface NO_x emissions from multi-constituent satellite data assimilation,
1068 Atmospheric Chem. Phys., 17, 807–837, https://doi.org/10.5194/acp-17-807-2017, 2017.

1069 Napelenok, S. L., Pinder, R. W., Gilliland, A. B., and Martin, R. V.: A method for evaluating
1070 spatially-resolved NOx emissions using Kalman filter inversion, direct sensitivities, and space-
1071 based NO2 observations, Atmos Chem Phys, 2008.

1072 Oo, T. K., Arunrat, N., Kongsurakan, P., Sereenonchai, S., and Wang, C.: Nitrogen dioxide
1073 (NO2) level changes during the control of COVID-19 pandemic in thailand, Aerosol Air Qual.
1074 Res., 21, 200440, https://doi.org/10.4209/aaqr.200440, 2021.

1075 Opio, R., Mugume, I., Nakatumba-Nabende, J., Nanteza, J., Nimusiima, A., Mbogga, M., and
1076 Mugagga, F.: Evaluation of WRF-chem simulations of NO2 and CO from biomass burning over
1077 east africa and its surrounding regions, Terr. Atmospheric Ocean. Sci., 33, 29,
1078 https://doi.org/10.1007/s44195-022-00029-9, 2022.

1079 Park, J., Jung, J., Choi, Y., Lim, H., Kim, M., Lee, K., Lee, Y., and Kim, J.: Satellite-based, top-
1080 down approach for the adjustment of aerosol precursor emissions over east asia: the
1081 geostationary environment monitoring spectrometer (GEMS) data fusion product and its proxies,
1082 https://doi.org/10.5194/egusphere-2023-87, 30 January 2023.

https://doi.org/10.5194/egusphere-2026-2309
Preprint. Discussion started: 20 May 2026

Park, J., Choi, Y., Jung, J., Lee, K., and Yeganeh, A. K.: First top-down diurnal adjustment to NOx emissions inventory in Asia informed by the Geostationary Environment Monitoring Spectrometer (GEMS) tropospheric NO2 columns, Sci. Rep., 14, 24338, https://doi.org/10.1038/s41598-024-76223-1, 2024.

Philip, S., Martin, R. V., Van Donkelaar, A., Lo, J. W.-H., Wang, Y., Chen, D., Zhang, L., Kasibhatla, P. S., Wang, S., Zhang, Q., Lu, Z., Streets, D. G., Bittman, S., and Macdonald, D. J.: Global chemical composition of ambient fine particulate matter for exposure assessment, Environ. Sci. Technol., 48, 13060–13068, https://doi.org/10.1021/es502965b, 2014.

Pinichka, C., Makka, N., Sukkumnoed, D., Chariyalertsak, S., Inchai, P., and Bundhamcharoen, K.: Burden of disease attributed to ambient air pollution in thailand: a GIS-based approach, PLOS ONE, 12, e0189909, https://doi.org/10.1371/journal.pone.0189909, 2017.

Poboon, C., Jongjaiphakdee, W., and Singkham, T.: Air pollution management in rayong's industrial area, thailand, AIR POLLUTION 2012, 189–199, https://doi.org/10.2495/AIR120171, 2012.

Pollution Control Department: สถานการณ์และการจัดการปัญหามลพิษทางอากาศและเสียง, 2022.

Qu, Z., Henze, D. K., Theys, N., Wang, J., and Wang, W.: Hybrid mass balance/4D-var joint inversion of NO_x and SO_2 emissions in east asia, J. Geophys. Res. Atmospheres, 124, 8203–8224, https://doi.org/10.1029/2018JD030240, 2019.

Seo, S., Kim, S.-W., Kim, K.-M., Richter, A., Lange, K., Burrows, J. P., Park, J., Hong, H., Lee, H., Jeong, U., and Kim, J.: Diurnal variations of NO_2 tropospheric vertical column density over the seoul metropolitan area from the geostationary environment monitoring spectrometer (GEMS): seasonal differences and impacts of varying a priori NO_2 profile data, https://doi.org/10.5194/amt-2024-33, 12 March 2024.

Souri, A. H., Nowlan, C. R., González Abad, G., Zhu, L., Blake, D. R., Fried, A., Weinheimer, A. J., Wisthaler, A., Woo, J.-H., Zhang, Q., Chan Miller, C. E., Liu, X., and Chance, K.: An inversion of NO_x and non-methane volatile organic compound (NMVOC) emissions using satellite observations during the KORUS-AQ campaign and implications for surface ozone over East Asia, Atmospheric Chem. Phys., 20, 9837–9854, https://doi.org/10.5194/acp-20-9837-2020, 2020.

Tang, W., Cohan, D. S., Lamsal, L. N., Xiao, X., and Zhou, W.: Inverse modeling of Texas NO_x emissions using space-based and ground-based NO_2 observations, Atmospheric Chem. Phys., 13, 11005–11018, https://doi.org/10.5194/acp-13-11005-2013, 2013.

Thawonkaew, A.: Assimilative capacity of air pollutants in an area of the largest petrochemical complex in thailand, Int. J. Geomate, https://doi.org/10.21660/2016.23.1177, 2016.

Thompson, A. M.: The oxidizing capacity of the earth's atmosphere: probable past and future changes, Science, 256, 1157–1165, https://doi.org/10.1126/science.256.5060.1157, 1992.

https://doi.org/10.5194/egusphere-2026-2309
Preprint. Discussion started: 20 May 2026

Thongsame, W., Henze, D. K., Kumar, R., Barth, M., and Pfister, G.: Evaluation of WRF-chem PM2.5 simulations in thailand with different anthropogenic and biomass-burning emissions, Atmospheric Environ. X, 23, 100282, https://doi.org/10.1016/j.aeaoa.2024.100282, 2024.

Turner, A. J., Henze, D. K., Martin, R. V., and Hakami, A.: The spatial extent of source influences on modeled column concentrations of short-lived species, Geophys. Res. Lett., 39, 2012GL051832, https://doi.org/10.1029/2012GL051832, 2012.

Uttamang, P., Aneja, V. P., and Hanna, A. F.: Assessment of gaseous criteria pollutants in the bangkok metropolitan region, thailand, Atmospheric Chem. Phys., 18, 12581–12593, https://doi.org/10.5194/acp-18-12581-2018, 2018.

Veefkind, J. P., Aben, I., McMullan, K., Förster, H., De Vries, J., Otter, G., Claas, J., Eskes, H. J., De Haan, J. F., Kleipool, Q., Van Weele, M., Hasekamp, O., Hoogeveen, R., Landgraf, J., Snel, R., Tol, P., Ingmann, P., Voors, R., Kruizinga, B., Vink, R., Visser, H., and Levelt, P. F.: TROPOMI on the ESA Sentinel-5 Precursor: A GMES mission for global observations of the atmospheric composition for climate, air quality and ozone layer applications, Remote Sens. Environ., 120, 70–83, https://doi.org/10.1016/j.rse.2011.09.027, 2012.

Watanabe, M., Oba, A., Saito, Y., Purevjav, G., Gankhuyag, B., Byamba-Ochir, M., Zamba, B., and Shishime, T.: Enhancing scientific transparency in national CO2 emissions reports via satellite-based a posteriori estimates, Sci. Rep., 13, 15427, https://doi.org/10.1038/s41598-023-42664-3, 2023.

Wiedinmyer, C., Kimura, Y., McDonald-Buller, E. C., Emmons, L. K., Buchholz, R. R., Tang, W., Seto, K., Joseph, M. B., Barsanti, K. C., Carlton, A. G., and Yokelson, R.: The fire inventory from NCAR version 2.5: an updated global fire emissions model for climate and chemistry applications, Atmospheric sciences, https://doi.org/10.5194/egusphere-2023-124, 2023.

Williams, J. E., Boersma, K. F., Le Sager, P., and Verstraeten, W. W.: The high-resolution version of TM5-MP for optimized satellite retrievals: description and validation, Geosci. Model Dev., 10, 721–750, https://doi.org/10.5194/gmd-10-721-2017, 2017.

Yang, L. H., Jacob, D. J., Dang, R., Oak, Y. J., Lin, H., Kim, J., Zhai, S., Colombi, N. K., Pendergrass, D. C., Beaudry, E., Shah, V., Feng, X., Yantosca, R. M., Chong, H., Park, J., Lee, H., Lee, W.-J., Kim, S., Kim, E., Travis, K. R., Crawford, J. H., and Liao, H.: Interpreting GEMS geostationary satellite observations of the diurnal variation of nitrogen dioxide (NO_2) over east asia, https://doi.org/10.5194/egusphere-2023-2979, 22 December 2023.

Yang, Y., Zhao, Y., Zhang, L., Zhang, J., Huang, X., Zhao, X., Zhang, Y., Xi, M., and Lu, Y.: Improvement of the satellite-derived NOx emissions on air quality modeling and its effect on ozone and secondary inorganic aerosol formation in the yangtze river delta, china, Atmospheric Chem. Phys., 21, 1191–1209, https://doi.org/10.5194/acp-21-1191-2021, 2021.

Zaveri, R. A., Easter, R. C., Fast, J. D., and Peters, L. K.: Model for simulating aerosol interactions and chemistry (MOSAIC), J. Geophys. Res., 113, D13204, https://doi.org/10.1029/2007JD008782, 2008.

https://doi.org/10.5194/egusphere-2026-2309
Preprint. Discussion started: 20 May 2026

1157 Zhang, L., Jacob, D. J., Knipping, E. M., Kumar, N., Munger, J. W., Carouge, C. C., Van
1158 Donkelaar, A., Wang, Y. X., and Chen, D.: Nitrogen deposition to the united states: distribution,
1159 sources, and processes, Atmospheric Chem. Phys., 12, 4539–4554,
1160 https://doi.org/10.5194/acp-12-4539-2012, 2012.

1161 Zhang, Y., Dubey, M. K., Olsen, S. C., Zheng, J., and Zhang, R.: Comparisons of WRF/chem
1162 simulations in mexico city with ground-based RAMA measurements during the 2006-MILAGRO,
1163 Atmospheric Chem. Phys., 9, 3777–3798, https://doi.org/10.5194/acp-9-3777-2009, 2009.

1164 Zhao, X., Griffin, D., Fioletov, V., McLinden, C., Cede, A., Tiefengraber, M., Müller, M., Bognar,
1165 K., Strong, K., Boersma, F., Eskes, H., Davies, J., Ogyu, A., and Lee, S. C.: Assessment of the
1166 quality of TROPOMI high-spatial-resolution NO_2 data products in the greater toronto area,
1167 Atmospheric Meas. Tech., 13, 2131–2159, https://doi.org/10.5194/amt-13-2131-2020, 2020.